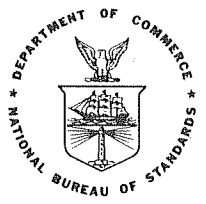

NBS TECHNICAL NOTE 1303

U.S. DEPARTMENT OF COMMERCE / National Bureau of Standards

A Lattice Approach to Volumes Irradiated by Unknown Sources

J. Randa
M. Kanda

A Lattice Approach to Volumes Irradiated by Unknown Sources

J. Randa
M. Kanda

Electromagnetic Fields Division
Center for Electronics and Electrical Engineering
National Engineering Laboratory
National Bureau of Standards
Boulder, Colorado 80303

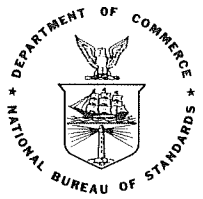

U.S. DEPARTMENT OF COMMERCE, Malcolm Baldrige, Secretary

NATIONAL BUREAU OF STANDARDS, Ernest Ambler, Director

Issued October 1986

National Bureau of Standards Technical Note 1303
Natl. Bur. Stand. (U.S.), Tech Note 1303, 64 pages (Oct. 1986)
CODEN: NBTNAE

U.S. GOVERNMENT PRINTING OFFICE
WASHINGTON: 1986

For sale by the Superintendent of Documents, U.S. Government Printing Office, Washington, DC 20402

CONTENTS

A LATTICE APPROACH TO VOLUMES IRRADIATED BY UNKNOWN SOURCES

J. Randa and M. Kanda

Electromagnetic Fields Division
National Bureau of Standards
Boulder, CO 80303

We suggest an approach to the characterization of electromagnetic environments irradiated by unknown sources. The approach is based on the numerical solution of Maxwell's equations subject to the constraints imposed by the measured values of the field at a small number of measurement points and by boundary conditions. A thorough examination of two methods for the numerical solution is presented. The examples attempted demonstrate the approach but reveal that neither numerical technique is fully successful. Possible future directions are suggested.

Key words: electromagnetic environment characterization; electromagnetic environment effects; Hamilton's action principle; ill-posed problems; numerical methods; successive over-relaxation method.

1. INTRODUCTION

As the number of intentional and inadvertent sources of electromagnetic (EM) radiation increases, the task of measuring and characterizing EM environments becomes increasingly difficult. At the same time more sensitive electronic devices are being used, and evidence is beginning to accumulate (see e.g. [1]) that the human body may be more sensitive to low-level nonionizing radiation than previously assumed. It is therefore increasingly important to develop methods to measure and characterize the EM environments in which devices and people are found.

The only systematic approach which has been developed and actually implemented is the statistical approach [2-4]. It has been developed quite thoroughly for applications to communications systems [5-7] and has been used in a wide variety of applications, including EM noise in mines [8], EM emissions from cars [9, 10] and trains [11], radio reception inside houses [12, 13], and characterization of urban environments [14-16]. Statistical methods are well suited to cataloguing general features of general environments, such as the average field level in a typical room of a generic suburban house. However, they require too many measurements to be efficient for specific characteristics and particular situations. (A directional scanning method which requires less measurement effort has been suggested [17], but it has not yet been fully developed.)

In this paper we address the question of how to efficiently extract information about a specific small to intermediate (several wavelength) size environment, e.g. the fields in one particular room rather than the average of many rooms. We assume some volume of interest which is free of primary sources, but which may contain conductors carrying induced currents. No knowledge of the source(s) irradiating the volume is assumed. Instead we

assume knowledge of the field at some number of measurement points. In principle the field measured can be the electric or magnetic field, or both; but in this paper we assume it is the electric field. If both were measured, it would require holding fixed spatial derivatives of the vector potential at measurement points, as well as the vector potential itself. We also restrict our attention to the single-frequency case. The extension to multiple frequencies could be effected through superposition, with a concomitant increase in measurement effort.

The basic idea of the method we consider is to attempt to numerically find an approximate solution to Maxwell's equations which is consistent with the measured values of the field at measurement points and which is also consistent with the appropriate boundary conditions at the surfaces of any conductors within or bounding the volume of interest. Although it is not the way in which the computation proceeds, one can think of the problem as being divided into two distinct steps. Since the geometry of a real situation may well be quite awkward, the normal modes of the system would not be known and would need to be determined. The second step would be to determine what combination of modes was consistent with the measurements. This second point merits some discussion. We are interested in obtaining information from as few measurements as possible, and therefore in the typical case there will be insufficient information to uniquely determine the field in the volume of interest. This raises two complications. Of the many possible solutions consistent with the measured values of the field, we must be able to always find the "same" one, the solution with some identifying feature (preferably a useful one). For example, we would want to always find the one with the largest (smallest) average energy density, or the most probable one, etc. The other complication is that, because there are many solutions, the matrix

equation obtained by discretizing the system involves a singular matrix. Consequently, methods requiring the inversion of that matrix are inapplicable.

In this paper we develop and illustrate the approach in some simple cases. The particular geometry chosen is a rectangular box with perfectly conducting walls. This example was obviously chosen for its simplicity rather than its practical relevance, but it is not so far removed from reality. Introduction of a few holes for windows and doors makes it a model of a metal building or room. Another simplification which we have already mentioned is the assumption that only one frequency is present.

We consider two different numerical techniques for finding solutions to Maxwell's equations subject to the constraint that the field assume specific values at the measurement points. Both methods first impose a spatial grid or lattice on the volume of interest and are formulated in terms of the field values at the lattice points. The first method employs Hamilton's principle and the action functional for classical electromagnetism. For field configurations which are solutions of Maxwell's equations, the action is stationary with respect to small variations of the field; and so the appropriate components of the field are fixed at boundaries, the field is fixed at the measured values at measurement points, and it is allowed to vary everywhere else until a stationary point of the action is found. The second numerical technique is to attempt a direct solution of the relevant differential equations, which are the vector Helmholtz equation supplemented by the condition that the divergence of the vector potential vanish. This can be considered an alternate approach to locating the stationary point of the action, since the action stationarity leads to Maxwell's equations and thence to the Helmholtz equation and divergence condition in our case. Again the field is set equal to measured values at measurement points, and the Helmholtz

equation and divergence condition are solved simultaneously using a successive over-relaxation (SOR) method. Neither of the two numerical methods is entirely successful, but the SOR method has enough success to demonstrate the general approach and to point out avenues for development.

In the next section we present the first numerical technique, based on the action functional. The SOR technique is applied to the Helmholtz equation and divergence condition in Section 3. In the final section we summarize the work and comment on future prospects.

2. STATIONARITY OF THE ACTION

2.1 Formulation

In terms of the usual vector and scalar potentials $\vec{A}(\vec{x},t)$ and $\phi(\vec{x},t)$, the action functional for classical (lossless) electromagnetism is [18, 19]

$$\mathcal{A} = \int_{t_1}^{t_2} dt \int d^3x \left\{\frac{1}{2}\left[\left(\vec{\nabla}\phi + \frac{\partial}{\partial t}\vec{A}\right) \cdot \overleftrightarrow{\varepsilon}(\vec{x}) \cdot \left(\vec{\nabla}\phi + \frac{\partial}{\partial t}\vec{A}\right)\right.\right. \tag{2.1}$$

$$\left.\left. - (\vec{\nabla} \times \vec{A}) \cdot \overleftrightarrow{\mu}^{-1}(\vec{x}) \cdot (\vec{\nabla} \times \vec{A}) + \vec{A} \cdot \vec{J}(\vec{x},t) - \phi\, \rho(\vec{x},t)\right\},$$

where $\overleftrightarrow{\varepsilon}$ and $\overleftrightarrow{\mu}$ are the permittivity and permeability, and $\vec{J}$ and ρ are the current and charge densities. The spatial integral extends over the volume of interest, subject to the restrictions imposed by the variations of the potentials vanishing on the surface (see below). We work with the potentials rather than the electric and magnetic fields because Hamilton's principle requires that the quantities being varied be independent degrees of freedom, whereas $\vec{E}$ and $\vec{H}$ are related. The four potentials $(\vec{A},\phi)$ cannot all be independent either, of course, but one can be easily eliminated when the gauge choice is made.

In this formulation, the two homogeneous Maxwell's equations follow immediately from the definition of $\vec{E}$ and $\vec{B}$ in terms of the potentials:

$$\left.\begin{aligned} \vec{E} &= -\left(\vec{\nabla}\phi + \frac{\partial}{\partial t}\vec{A}\right) \\ \vec{B} &= \vec{\nabla} \times \vec{A} \end{aligned}\right\} \longrightarrow \begin{aligned} &\vec{\nabla} \times \vec{E} + \frac{\partial}{\partial t}\vec{B} = 0 \\ &\vec{\nabla} \cdot \vec{B} = 0 \quad . \end{aligned} \tag{2.2}$$

The two remaining Maxwell's equations follow from Hamilton's principle [10]. If we consider small variations of the potentials and requires that the resulting variation of the action vanish, we obtain

$$\begin{aligned} &\delta_{\phi} \mathcal{A} = 0 \rightarrow \vec{\nabla} \cdot \vec{D} = \rho, \\ &\delta_{\vec{A}} \mathcal{A} = 0 \rightarrow \vec{\nabla} \times \vec{H} - \frac{\partial}{\partial t}\vec{D} = \vec{J}, \end{aligned} \tag{2.3}$$

provided the variations of $\vec{A}$ and ϕ vanish at the end points. To be more exact, what is required is that $\delta\phi$ and $\delta\vec{A}$ vanish on the surface of the volume V at all times and that $\delta\vec{A}$ vanish throughout the volume at times t_1 and t_2. What this means in practice is that in order to use this in a calculation, we must specify the fields on the boundary surface at all times and throughout the volume at the initial and final times. In any real application, such a superabundance of information will not be available for the volume of interest. In order to exploit the stationarity of the action we must expand the volume considered beyond the region of interest, out to distances where the fields can be assumed to be negligible. The same applies to the time; t_1 is chosen before the fields are turned on and t_2 after they are turned off.

For the calculations that follow, it will be convenient to work in a definite gauge. A propitious choice is $\phi(\vec{x},t) = 0$. The action then assumes the form

$$\mathcal{A} = \int dt \int d^3x \left\{\frac{1}{2}\left[\left(\frac{\partial}{\partial t}\vec{A}\right) \cdot \overleftrightarrow{\varepsilon} \cdot \left(\frac{\partial}{\partial t}\vec{A}\right) - \left(\vec{\nabla} \times \vec{A}\right) \cdot \overleftrightarrow{\mu}^{-1} \cdot \left(\vec{\nabla} \times \vec{A}\right)\right] + \vec{A} \cdot \vec{J}\right\}. \tag{2.4}$$

This gauge has the convenient feature that for the single-frequency case a measurement of the electric field directly determines $\vec{A}$, $\vec{E}(\vec{x},t) = \omega \vec{A}(\vec{x},t - \pi/2\omega)$.

Having extended the volume under consideration to virtually all of space-time, we must restrict the problem to manageable size. In particular, since we do not know the sources, the volume of interest is chosen to exclude them. We envision the division depicted in Fig. 2-1. The volume marked V_I is the region of interest; it is assumed to be free of primary sources, but it may contain conductors with induced currents. Volume V_B is a buffer zone separating V_I from V_S, which is the rest of space, wherein are located any primary sources. The idea is to divide the action into one piece from the integral over volumes V_I and V_B and another piece from V_S. Because V_S contains unknown sources, we do not try to determine the fields there, which means that we also will not know the fields on the surface between V_S and V_B. The fields on that surface will be allowed to vary or will be fixed by a reasonable guess. Obviously, near the boundary between V_S and V_B the solution obtained will be very sensitive to the choice for the fields on that boundary, and therefore it will not be reliable. As we move away from the outer boundary of V_B the values of the fields should be influenced more by the measurement points and less by the values on the surface between V_S and V_B. For points far enough away from that surface--i.e. within V_I--it should be

possible to obtain reliable solutions, given enough measurement points. The hope is that "far enough away" and "enough points" are not so large as to render the method impractical for most applications. The positions of the measurement points will clearly affect the size required for V_B; it may well be advantageous to make a few measurements on the perimeter of V_B. It would probably also be advisable to choose the boundary of V_B to coincide with conducting walls when it is feasible, in order to constrain the fields on the boundary as much as possible.

The quantity we shall consider then is a reduced action, $\hat{a}$, which is defined as in eq. (2.4) but with the integral restricted to $V_I \oplus V_B$. (In the general multiple-frequency case the volumes are four-dimensional space-time volumes.) The next step is to discretize the expression for the reduced action, converting the volume integral into a summation which approximates it. There are any number of ways to do so; we are not interested in their relative (dis)advantages at this time. The discretized reduced action will have the general form

$$\hat{a} = \int dt \sum_{\alpha,\beta,\gamma \epsilon V_I \oplus V_B} \Delta V_{\alpha\beta\gamma} \frac{1}{2} \{ \left(\frac{\partial}{\partial t} \vec{A}(t)\right)_{\alpha\beta\gamma} \cdot \overleftrightarrow{\varepsilon}_{\alpha\beta\gamma} \cdot \left(\frac{\partial}{\partial t} \vec{A}(t)\right)_{\alpha\beta\gamma} \tag{2.5}$$

$$- \left(\vec{\nabla} \times \vec{A}(t)\right)_{\alpha\beta\gamma} \cdot \overleftrightarrow{\mu}^{-1}_{\alpha\beta\gamma} \cdot \left(\vec{\nabla} \times \vec{A}(t)\right)_{\alpha\beta\gamma} \} .$$

The discrete indices α,β,γ label the spatial points, on which are centered the volume elements $\Delta V_{\alpha\beta\gamma}$. We have left the time variable continuous for now, anticipating the single-frequency example below. The quantities $(\partial\vec{A}/\partial t)_{\alpha\beta\gamma}$ and $(\vec{\nabla} \times \vec{A})_{\alpha\beta\gamma}$ will in general depend on the values of the

field $\vec{A}$ at a number of points on (or within) the surface bounding $\Delta V_{\alpha\beta\gamma}$. A concrete realization of this discretization of $\hat{a}$ will be given in the example below. Imposition of the constraints required by the known values of $\vec{E}$ and/or $\vec{H}$ at measurement points can be rather complicated, but for only one frequency and for our gauge choice $\vec{E}_{\alpha\beta\gamma} \propto \vec{A}_{\alpha\beta\gamma}$, and a measurement of the electric field at a point fixes $\vec{A}_{\alpha\beta\gamma}$ at that point. A similar comment applies to boundary conditions at perfectly conducting walls; for the single-frequency case they can be imposed with relative ease.

The calculation then proceeds as follows. A grid is defined within $V_B \oplus V_I$, and $\vec{A}_{\alpha\beta\gamma}$ is fixed at measurement points and appropriate components are set equal to zero at conducting walls. All other $\vec{A}_{\alpha\beta\gamma}$'s are varied, and we search numerically for a stationary point of $\hat{a}$ in eq.(2.5). When (if) a stationary point is found, then that set of $\vec{A}_{\alpha\beta\gamma}$ constitutes an approximate solution to Maxwell's equations within $V_B \oplus V_I$ which is consistent with measured field values and boundary conditions. The problem of finding the stationary point is nontrivial, however, and we now turn our attention to that.

2.2 Nature of the Stationary Point and the Euclidean Action

The technique presented in this paper depends on finding field configurations such that the action is stationary with respect to small variations of the field. Such field configurations are solutions of Maxwell's equations. The standard method of finding the stationary point would be to discretize the functional as in (2.5), set $\partial a / \partial A^i_{\alpha\beta\gamma} = 0$ to obtain a (large) matrix equation, and solve that equation. That approach founders here because the matrix would be (very) singular. There are in general many possible solutions consistent with boundary conditions, measured fields, and unknown sources. We need to locate a stationary point and to know which

stationary point it is--does it correspond to the solution with the largest maximum electric field in the volume, or the solution with the minimum power density, etc. To locate the stationary points numerically we need to know whether they are maxima, minima, or neither. The phrase "Principle of Least Action" may lead one to expect a minimum, but in general this need be true only for infinitesimal time intervals $\Delta t \equiv t_2 - t_1$. To consider our specific case, we adapt the treatment of Whittaker [20]. We use the form of eq. (2.4) and assume for simplicity that $\overleftrightarrow{\varepsilon}$ and $\overleftrightarrow{\mu}^{-1}$ are scalar constants. If the fields are allowed to vary

$$\vec{A}(\vec{x},t) \to \vec{A}(\vec{x},t) + \vec{\alpha}(\vec{x},t), \qquad \vec{\alpha}(\vec{x},t_1) = \alpha(\vec{x},t_2) = 0, \tag{2.6}$$

where $\vec{\alpha}$ is small, then the second-order variation of the action is

$$\delta^2 \mathcal{A} = \frac{1}{2} \int_{t_1}^{t_2} dt \int d^3x \left[\varepsilon \dot{\vec{\alpha}}^2 - \frac{1}{\mu} (\vec{\nabla} \times \vec{\alpha})^2 \right]. \tag{2.7}$$

The usual argument is that because $\vec{\alpha}$ but not $\dot{\vec{\alpha}}$ vanishes at t_1 and t_2, for small $t_2 - t_1$ the first term dominates the integral in (2.7) and the stationary point is a minimum. That argument fails in a field theory, however, where the second term involves spatial derivatives of the dynamical variables. Because the functional form of $\vec{\alpha}(\vec{x},t)$ is arbitrary, its spatial dependence can oscillate wildly and $\delta^2 \mathcal{A}$ can be positive or negative (depending on the choice of $\vec{\alpha}$) for any fixed nonzero Δt. Therefore the stationary points of are neither maxima nor minima.

This changes when the action is discretized by the introduction of a spatial grid. Then the spatial derivatives of $\vec{\alpha}$ are bounded by $(\vec{\nabla} \times \vec{\alpha})^2 \lesssim O(\vec{\alpha}^2/a^2)$, where a is the lattice spacing. The stationary point is a minimum provided Δt is less than some number on the order of $\sqrt{\varepsilon\mu}\,a$. For

larger values of Δt, $\delta^2 \mathcal{A}$ can again have either sign, and consequently the minimum is again a saddle point. That is the case of interest since we need $\Delta t \to \infty$ in order to set all the fields equal to zero at t_1 and t_2.

This poses a serious calculational problem. A stationary point which is neither a maximum nor a minimum will be very difficult to locate numerically. In earlier work [21, 22] we introduced a method which succeeded in some simple cases, but subsequent tests with more complex field configurations (i.e. higher modes) have exposed inadequacies in that method. Faced with the impracticality of numerically locating saddle points of functions of very many (10^3-10^6) variables, we need a function to maximize or minimize. Our efforts to construct such a function have not been marked by complete success. One interesting attempt which was partially successful is to borrow a trick from quantum field theory and work in Euclidean space-time [23]. To do so we take time to be imaginary, $t = -i\tau$ with τ real, thereby changing the sign of the $(\partial \vec{A}/\partial t)^2$ term in (2.5) and (2.7). We solve the problem in Euclidean space and analytically continues the result back to Minkowski space, $\tau \to it$. The Euclidean action is

$$\mathcal{A}_E = \int_{\tau_1}^{\tau_2} d\tau \int d^3x \left\{ \frac{1}{2} \left(\frac{\partial}{\partial \tau} \vec{A}_E(\vec{x},\tau) \right) \cdot \overleftrightarrow{\varepsilon} \cdot \left(\frac{\partial}{\partial \tau} \vec{A}_E \right) \right. \tag{2.8}$$

$$\left. + \frac{1}{2} \left(\vec{\nabla} \times \vec{A}_E \right) \cdot \overleftrightarrow{\mu}^{-1} \cdot \left(\vec{\nabla} \times \vec{A}_E \right) - \vec{A}_E \cdot \vec{J} \right\} ,$$

and this is to be minimized to obtain the physical solutions in Euclidean space. The analytic continuation back to Minkowski space can be a difficulty in general, and in fact it will prove to be the limiting factor for this technique. Nevertheless, it is possible to handle some simple examples in this manner.

As noted above, there will be many possible solutions consistent with a few field measurements if the sources are unknown. The Euclidean solution is obtained by minimizing the integral of the energy density $(\frac{1}{2}\,\varepsilon\,\vec{E}_E^2 + \frac{1}{2}\,\mu\,\vec{H}_E^2)$. As will be seen below, for the single frequency case this also corresponds to minimizing the energy density in Minkowski space. Therefore, the solution obtained will be the one with the minimum average energy density in the volume under consideration. This is a welcome bonus of working in Euclidean space--not only can we find a solution, but it is a useful one as well.

The entire procedure, including the analytic continuation and numerical search method, is greatly clarified by an example, to which the next subsection is devoted.

2.3 Simple Example

A. Problem and Calculation

Having presented the general ideas of this approach, we now attempt to implement it in a simple example--a rectangular waveguide with perfectly conducting walls. This is obviously not supposed to be a practical application, and many of the difficulties and nuances of the general case are absent. It is a practice problem to demonstrate the idea and to provide a basis on which to build toward solution of real problems. The rectangular waveguide is chosen because it has simple known modes, because the boundary conditions are easily imposed, and because it can be reduced to a two-(or even one-) dimensional problem, thereby reducing the computational exercise. As we shall see below, even in this simple case, it is not entirely trivial to obtain the correct continuum answer, with which to compare the results of our numerical computation.

We first restrict the problem to two dimensions, obtaining the general forms for $\vec{A}_E$ and $\vec{A}_M$ (the vector potentials in Euclidean and Minkowski space, respectively) and the relationship between them. To facilitate the analytic continuation, we assume a standing wave due to perfect reflection from the (very distant) end of the waveguide. For a given TE mode, TE_{mn}, $\vec{A}_M$ can then be written

$$\vec{A}_M(\vec{x},t) = \vec{A}(\vec{x}_\perp) \cos kz \cos \omega t \equiv \vec{A}(\perp) \cos kz \cos \omega t, \tag{2.9}$$

$$k = \sqrt{\frac{\omega^2}{c^2} - \pi^2 \left(\frac{m^2}{a^2} + \frac{n^2}{b^2}\right)},$$

where a and b are the transverse dimensions of the waveguide ($a \geq b$), c is the speed of light in the waveguide medium, $\vec{x}_\perp = (x,y)$ is the two-dimensional transverse position vector, and $\vec{A}_M(\vec{x},t)$ and $\vec{A}(\perp)$ are real. Equation (2.9) would allow a simple restriction to two dimensions for a single mode. However, the solutions of interest are those with the minimum energy density consistent with the measurements, and those solutions are superpositions of many modes. Consequently the true solution will not have a z dependence which can be factored out as in (2.9), and the problem will not reduce to two dimensions. In order to force it to do so, we impose the form of eq (2.9) with k taken to be that of the lowest mode consistent with the measurements. That yields a two-dimensional problem, but it is no longer electromagnetism: if the solutions $\vec{A}(\perp)$ are substituted back into (2.9), the resulting $\vec{A}(\vec{x},t)$ need not be a solution of Maxwell's equations. Nonetheless, the action and the problem are quite similar to electromagnetism, and it is a suitable problem for demonstration purposes since one can obtain the true solutions for comparison. This arbitrarily imposed z dependence does not reflect a

shortcoming of the method, but rather the difficulty of finding a simple two-dimensional application.

To obtain the general form for $\vec{A}_E$, we require that it be real and that it satisfy the Euclidean wave equation

$$\left(\vec{\nabla}^2 + \mu\varepsilon \frac{\partial^2}{\partial\tau^2}\right) \vec{A}_E(\vec{x},\tau) = 0 \ . \tag{2.10}$$

It can then be written as

$$\begin{aligned}\vec{A}_E\ (\vec{x},\tau) = {} & \vec{a}_E(\perp)\ e^{i(kz + \bar{\omega}\tau)} + \vec{b}_E(\perp)\ e^{i(kz - \bar{\omega}\tau)} \\ & + \vec{c}_E(\perp)\ e^{-i(kz + \bar{\omega}\tau)} + \vec{d}_E(\perp)\ e^{-i(kz - \bar{\omega}\tau)} + \text{compl. conj.},\end{aligned} \tag{2.11}$$

where $\bar{\omega}$ need not be (in fact is not) real. If (2.11) is then continued back to Minkowski space ($\tau = it$) and compared to (2.9), the relation between $\vec{A}_E$ and $\vec{A}_M$ follows. We can write

$$\vec{A}_E\ (\vec{x},\tau) = \vec{A}(\perp)\ \cos kz\ \cosh \omega\tau, \tag{2.12}$$

where $\vec{A}(\perp)$, k, and ω are the same as in (2.9). Equation (2.12) enables us to use measurements of $\vec{A}_M$ to constrain $\vec{A}_E$. Conversely once $\vec{A}_E$ is determined by the computation, $\vec{A}(\perp)$ and hence also $\vec{A}_M$ are known.

Substituting the form for $\vec{A}_E$ (2.12) into the Euclidean action (2.8) leads to

$$\begin{aligned}a_E = C \int_{-\Delta}^{a+\Delta} dx \int_{-\Delta}^{b+\Delta} dy\ \{ & \left(\frac{\omega^2}{c^2} + k^2\right) \left[A_y^2(\perp) + A_x^2(\perp)\right] + \frac{\omega^2}{c^2} A_z^2(\perp) \\ & + \left[\left(\partial_y A_z(\perp)\right)^2 + \left(\partial_x A_z(\perp)\right)^2 + \left(\partial_x A_y(\perp) - \partial_y A_x(\perp)\right)^2\right] \\ & - 2\mu\ \vec{J}(\perp) \cdot \vec{A}(\perp)\},\end{aligned} \tag{2.12}$$

where $\vec{J}(\perp)$ is defined in terms of the wall current $\vec{J}(\vec{x},t)$ in the obvious way (9), and where the constant C is given by

$$C = \frac{1}{2\mu} \int_{\tau_1}^{\tau_2} d\tau \cosh^2 \omega t \int dz \cos^2 kz. \tag{2.14}$$

In writing (2.13) we have assumed that the material in the waveguide is isotropic and that the range of the z integration is either very long or an integral number of cycles. The induced current and the limits of the transverse integrations require explanation. In applying Hamilton's principle the variations of $\vec{A}$ must be zero on the boundary, which in our two-dimensional case here means that we must specify $\vec{A}$ on the transverse boundary. In order to be able to specify all components of $\vec{A}$ we choose the boundary to lie a few skin depths within the conducting walls where the field can safely be assumed to vanish. In figure 2-2 the x integration goes from $x = -\Delta$ to $x = a + \Delta$, and the y integration from $-\Delta$ to $b + \Delta$, where $\Delta \equiv N\delta$, some suitable number of skin depths. Then, however, the currents induced in the walls are contained within the integration volume. Fortunately, we can show that the contribution to the action from the volume within the conductor is negligible, and we can write

$$\mathcal{A}_E \simeq C \int_0^a dx \int_0^b dy \left\{ \left(\frac{\omega^2}{c^2} + k^2\right) \left[A_y^2(\perp) + A_x^2(\perp)\right] + \frac{\omega^2}{c^2} A_z^2(\perp) \right. \tag{2.15}$$

$$\left. + \left[(\partial_y A_z(\perp))^2 + (\partial_x A_z(\perp))^2 + (\partial_x A_y(\perp) - \partial_y A_x(\perp))^2\right]\right\}.$$

We still need to impose $\vec{E}_{tan} = 0$ and $\vec{B}_{norm} = 0$ at the conductor walls, which is accomplished by the requirements that $\vec{A}(\perp)_{tan}$ vanish at the walls.

The action is then discretized by introducing a rectangular grid into the waveguide as indicated in Fig. 2-3. The spacing between points is $\Delta x = a/N_x$, $\Delta y = b/N_y$. Derivatives at a point (i,j) are defined by

$$\left(\frac{\partial}{\partial x} A\right)_{ij} = \frac{A(i+1,j) - A(i,j)}{\Delta x} , \tag{2.16}$$

except at the boundaries, where

$$\left(\frac{\partial}{\partial x} A\right)_{N_x,j} \quad \left(\frac{\partial}{\partial x} A\right)_{N_x-1,j} , \tag{2.17}$$

and similarly for y derivatives. The Euclidean action then takes the form

$$\begin{aligned} a_E \simeq c \sum_{i=0}^{N_x} \sum_{j=0}^{N_y} \Delta A_{ij} \{ & [A_x(i,j)^2 + A_y(i,j)^2] c_{mn}\pi^2 \\ & + 4\pi^2 A_z(i,j)^2 + [(A_z(i,j+1) - A_z(i,j))/\Delta y]^2 \\ & + [(A_z(i+1,j) - A_z(i,j))/\Delta x]^2 + [(A_x(i,j+1) - A_x(i,j))/\Delta y \\ & - (A_y(i+1,j) - A_y(i,j))/\Delta x]^2 \}, \\ & c_{mn} = \left(8 - \frac{m^2}{a^2} - \frac{n^2}{b^2}\right) , \end{aligned} \tag{2.18}$$

where all lengths are in units of the free-space wavelength λ. The area elements are

$$\begin{aligned} \Delta A_{kl} &= \Delta x \, \Delta y \qquad 0<k,l<N \\ &= \tfrac{1}{2}\Delta x \, \Delta y \qquad k \text{ or } l = 0 \text{ or } N, \end{aligned} \tag{2.19}$$

and the "out of bounds" fields are defined as

$$\begin{aligned} \vec{A}(i,N_y + 1) &= 2\vec{A}(i,N_y) - \vec{A}(i,N_y - 1), \\ \vec{A}(N_x + 1, j) &= 2\vec{A}(N_x,j) - \vec{A}(N_x - 1,j). \end{aligned} \tag{2.20}$$

Having discretized the problem, we next set the values of the tangential fields to zero on the boundaries, set the fields equal to their measured values at measurement points, and vary all other fields to minimize a_E in

(2.18). The manner in which we minimize $\mathcal{A}_E$ is to step through the grid, at each point (i,j) setting the fields equal to the value required by $\partial \mathcal{A}_E / \partial A_a(i,j) = 0$, a = 1-3, given the current values of the field at neighboring points. This process is repeated until the action reaches a minimum and does not change significantly during further passes through the grid. (This is just the Gauss-Seidel method; see e.g. [24].)

B. Demonstration

To further demonstrate the method and to clarify the sort of solution obtained, we present a simple one-dimensional computation and compare it to the continuum results. The field was fixed at three measurement points,

$$A_y\ (\tfrac{a}{4},\tfrac{b}{2}) = 0.707,\ A_y\ (\tfrac{a}{2},\tfrac{b}{2}) = 1.0,\ A_y\ (\tfrac{3a}{4},\tfrac{b}{2}) = 0.707, \tag{2.21}$$

with A_x and A_z equal to zero at all three points. This field pattern corresponds to the TE_{10} mode, or any number of higher modes. The waveguide dimensions were taken to be a = 2.0, b = 1.0. The computation to find the minimum is straightforward and proceeds as outlined at the end of the previous subsection. Obtaining an analytical result for comparison is less trivial. To do so for the three-measurement case, we assume the y dependence of all fields is a constant and expand

$$A_y(x) = \sum_{j=1}^{\infty} a_j \sin(j\tfrac{\pi x}{a}). \tag{2.22}$$

A_x and A_z are zero at the measurement points and are therefore zero everywhere for the minimum-$\mathcal{A}_E$ solution. In terms of the a_j of (2.22) the action is

$$\mathcal{A}_E = C\,\frac{ab\pi^2}{8} \sum_j a_j^2(31 + j^2). \tag{2.23}$$

The constraints of (2.21) can be combined to yield

$$a_1 + \sum_{n=1}^{\infty} (a_{8n+1} - a_{8n-1}) = 1, \tag{2.24}$$

and two other constraints which lead to all a_i which do not contribute to (2.24) being zero.

In order to minimize $\mathcal{A}_E$ (2.23) subject to the constraint (2.24) we first use the constraint to eliminate a_1 and then set derivatives of $\mathcal{A}_E$ with respect to all other a_i equal to zero. This yields the infinite dimensional matrix equation

$$\begin{bmatrix} \Lambda_1^- & 1 & 1 & 1 \ldots \\ 1 & \Lambda_1^+ & 1 & 1 \ldots \\ 1 & 1 & \Lambda_2^- & 1 \ldots \\ 1 & 1 & 1 & \Lambda_2^+ \ldots \\ \cdot & \cdot & \cdot & \cdot \\ \cdot & \cdot & \cdot & \cdot \\ \cdot & \cdot & \cdot & \cdot \end{bmatrix} \begin{bmatrix} b_1^- \\ b_1^+ \\ b_2^- \\ b_2^+ \\ \cdot \\ \cdot \\ \cdot \end{bmatrix} = \begin{bmatrix} 1 \\ 1 \\ 1 \\ 1 \\ \cdot \\ \cdot \\ \cdot \end{bmatrix}, \tag{2.25}$$

where

$$b_n^{\pm} = \pm a_{8n\pm1},$$

$$\Lambda_n^{\pm} = 2 + 2n^2 \pm n/2. \tag{2.26}$$

This system can be solved by subtracting each row from the first to get the relation

$$b_n^{\pm} = \frac{\Lambda_1^- - 1}{\Lambda_n^{\pm} - 1} b_1^-. \tag{2.27}$$

The first row of (2.25) then determines b_1^-, and a_1 can be determined from (2.24). The result is

$$a_{8n\pm1} = \pm \frac{1}{\Lambda_n^{\pm} - 1} a_1, \quad n>0, \tag{2.28}$$

$$a_1 = \left[1 + \sum_{n=1}^{\infty} \left(\frac{1}{\Lambda_n^- - 1} + \frac{1}{\Lambda_n^+ - 1}\right)\right]^{-1}$$

$$= \frac{4\pi}{\sqrt{31}} \tanh\left(\frac{\pi}{4}\sqrt{31}\right) \simeq 0.43530.$$

Equation (2.28) and the fact that all other $a_i = 0$ can then be used in (2.22) to determine the true solution to which to compare the result of the numerical computation. Figure 2-4 shows the comparison, and it is obvious that a) the two sets of results agree with each other, and b) they agree with the measured values at x = a/4, a/2, and 3a/4.

2.4 Comments

The simple application in the preceding subsection illustrates both the general lattice approach to complex environment characterization and the attempt to implement this approach using Hamilton's principle and the action in Euclidean space-time. The example demonstrates that the lattice computation does produce the correct results. It indicates that in one dimension, for a system very similar to Maxwell's equations, we are able to find the minimum-energy-density solution consistent with measured field values at a few points, without knowledge of the external sources.

Unfortunately, a fundamental obstacle arises when less trivial examples are attempted. If there is any spatial variation in the phase of the field, or if the different components of the vector potential are not all in phase with each other, it becomes impossible to perform the analytic continuation as required. Since we are taking $\vec{A}$ to be real, phase variation appears as an admixture of cos ωt and sin ωt time dependences. One cannot continue both cos

and sin to imaginary time and still maintain the reality of $\vec{A}$ (which is necessary in order to keep the Euclidean action positive definite). Consequently, it does not appear that the trick of analytically continuing to imaginary time will be applicable in practical problems.

That leaves us with the problem of finding a stationary point of the action which is neither a maximum nor a minimum. Until that numerical problem can be solved, the action-based approach holds little promise.

3. DIFFERENTIAL EQUATION SOLUTION

3.1 Method

As in the preceding section we assume a single frequency, and we continue to choose the gauge so that the scalar potential vanishes. We then have

$$\begin{aligned} &\phi(\vec{x},t) = 0, \quad \vec{A}(\vec{x},t) = \vec{A}(\vec{x})\, e^{-i\omega t}, \\ &\vec{E}(\vec{x}) = i\omega\, \vec{A}(\vec{x}), \quad \vec{B}(\vec{x}) = \vec{\nabla} \times \vec{A}(\vec{x}). \end{aligned} \tag{3.1}$$

Equation (3.1) guarantees that E and B will satisfy the two homogeneous Maxwell equations. In a sourceless region of free space the two remaining Maxwell equations can be written

$$\vec{\nabla} \cdot \vec{A}(\vec{x}) = 0, \tag{3.2a}$$

$$\vec{\nabla}^2\, \vec{A}(x) + \omega^2 \mu\varepsilon\, \vec{A}(\vec{x}) = 0. \tag{3.2b}$$

We continue to measure all distances in units of the free space wavelength $\lambda = 2\pi/(\omega \sqrt{\mu\varepsilon})$, so that $\omega^2\mu\varepsilon = 4\pi^2$ in (3.2b).

The method presented in this section is to discretize the differential equations of (3.2) and then attempt to numerically solve them simultaneously subject to the constraint that the field is fixed at measurement points. Using finite difference forms for the derivatives, eqs (3.2a) and (3.2b) become

$$A_x(i+1,j,k) - A_x(i-1,j,k) + A_y(i,j+1,k) - A_y(i,j-1,k) + A_z(i,j,k+1) - A_z(i,j,k-1) = 0 \quad (3.3a)$$

$$[\vec{A}(i+1,j,k) + \vec{A}(i-1,j,k) + \vec{A}(i,j+1,k) + \vec{A}(i,j-1,k) + \vec{A}(i,j,k+1) + \vec{A}(i,j,k-1) - 6\,\vec{A}(i,j,k)]/\Delta^2 + 4\pi^2\,\vec{A}(i,j,k) = 0, \quad (3.3b)$$

where we have introduced a rectangular grid with equal spacing Δ in x,y, and z, and the positions of grid points are given by $(x,y,z) = (i,j,k)\Delta$. As in the previous section the cavity will have dimensions a,b,c, and $(N_x,N_y,N_z) = (a,b,c)/\Delta$ are the number of intervals in each direction. Points on the boundaries require special treatment since they lack neighbors in one or more directions. There we use the equation at the neighboring interior point. For example, the field at a point $(a,y,z) = (N_x,j,k)\Delta$ is determined from

$$A_x(N_x,j,k) - A_x(N_x-2,j,k) + A_y(N_x-1,j+1,k) - A_y(N_x-1,j-1,k) + A_z(N_x-1,j,k+1) - A_z(N_x-1,j,k-1) = 0, \quad (3.4a)$$

$$[\vec{A}(N_x,j,k) + \vec{A}(N_x-2,j,k) + \vec{A}(N_x-1,j+1,k) + \vec{A}(N_x-1,j-1,k) + \vec{A}(N_x-1,j,k+1) + \vec{A}(N_x-1,j,k-1) - 6\vec{A}(N_x-1,j,k)]/\Delta^2 + 4\pi^2\,\vec{A}(N_x-1,j,k) = 0. \quad (3.4b)$$

In general there will be more than one possible solution. A unique solution would require measurements at sampling theorem separations ($\leq \lambda/2$ for infinite free space), or knowledge of the sources, or knowledge of $\vec{A}$ on the boundary surface of the volume. This restricts the range of numerical methods available. To see this, consider just the vector Helmholtz equation, (3.3b). By arranging all field components $A_x(i,j,k)$, $A_y(i,j,k)$, $A_z(i,j,k)$ into one long vector z, one can put (3.3b) into the form of a matrix equation $Bz = 0$. Those elements of z corresponding to measurement or boundary points are known and can be brought over to the right hand side to yield an equation of the form $Ax = b$. If there is more than one solution, then A is singular and any method requiring the existence of A^{-1} will fail.

This leads us to adopt an iterative technique--the successive over-relaxation (SOR) method [24]. For simplicity, consider first just the vector Helmholtz equation, (3.3b). To apply SOR to this we step through the grid, and at each point (i,j,k) we first compute the residual, defined by

$$\vec{R}_H(i,j,k) \equiv \vec{A}(i,j,k) - [\vec{A}(i+1,j,k) + \vec{A}(i-1,j,k) + \vec{A}(i,j+1,k) + \vec{A}(i,j-1,k) + \vec{A}(i,j,k+1) + \vec{A}(i,j,k-1)]/(6 - 4\pi^2\Delta^2). \tag{3.5}$$

(This is actually the residual divided by $(6 - 4\pi^2\Delta^2)$, but we shall call it the residual.) We then change the vector potential at that point according to

$$\vec{A}'(i,j,k) = \vec{A}(i,j,k) - \Omega_H \vec{R}_H(i,j,k), \tag{3.6}$$

where Ω_H is a number between 0 and 2, chosen to optimize the rate of convergence. For $\Omega_H = 1$, this is the Gauss-Seidel method, in which the function $(\vec{A})$ is set equal to the value required to satisfy the difference equation(3.3b), given the current values of the function at neighboring points. For Ω_H greater (less) than one, the method is one of over-(under-) relaxation. The term SOR is used generically to apply to both over and under relaxation (and Gauss-Seidel as well) [24].

Application of the SOR method to the divergence condition (3.3a) is somewhat different due to the fact that (3.3a) relates different components of $\vec{A}$ at different points, and we would like to treat all three components the same. This can be accomplished in the following manner. We define the residual as

$$R_\nabla(i,j,k) \equiv -A_x(+) + A_x(-) - A_y(+) + A_y(-) - A_z(+) + A_z(-), \tag{3.7}$$

where

$$\begin{aligned} A_x(\pm) &= A_x(i \pm 1,j,k), \\ A_y(\pm) &= A_y(i,j \pm 1,k), \\ A_z(\pm) &= A_z(i,j,k \pm 1). \end{aligned} \tag{3.8}$$

The relaxation is then performed by spreading the residual equally over the $A_a(\pm)$'s,

$$A_x'(\pm) = A_x(\pm) \pm \frac{1}{6}\ \Omega_\nabla\ R_\nabla(i,j,k),$$

$$A_y'(\pm) = A_y(\pm) \pm \frac{1}{6}\ \Omega_\nabla\ R_\nabla(i,j,k), \qquad (3.9)$$

$$A_z'(\pm) = A_z(\pm) \pm \frac{1}{6}\ \Omega_\nabla\ R_\nabla(i,j,k),$$

where the relaxation parameter $\Omega_\nabla\ \varepsilon(0,2)$ is again chosen to optimize convergence.

We have discussed separately the SOR method for the vector Helmholtz equation and for the divergence condition, but in practice we want to solve the two simultaneously. This is done in the obvious manner: at each point (i,j,k) we first perform the divergence relaxation (3.9), thereby changing the field at neighboring points, and then perform the Helmholtz relaxation (3.6), changing the field at (i,j,k).

One final point we need to address before proceeding to examples is the question whether this procedure converges. It does not. Considering just the Helmholtz equation, even when all the boundary values are specified so that there is a unique solution, SOR can be shown not to converge [24,25]. The reason can be seen heuristically from eqs (3.5,3.6). For simplicity consider $\Omega_H = 1$ (Gauss-Seidel). Then if the sign of $4\pi^2\Delta^2$ were positive in the denominator, SOR would replace the value of the field at a point by a number somewhat smaller than the average of the field at neighboring points, and the process would converge. With the negative sign, however, the field at the point is replaced by a value larger than the average of neighboring values, and the process does not converge--the fields just keep growing.

Why then do we use it? There are two reasons. The first is that it is still possible to obtain approximate solutions by truncating the procedure at some point even if it does not converge. If we monitor the volume average of the residual, we can use as our result the field configuration corresponding to the minimum average residual. This truncated SOR will be used in the next subsections, with some success. The other reason for using this rather suspect procedure is that there is not an obviously better one available which suits our needs--i.e. does not require inversion of a singular matrix in the problems of interest. The (scalar or vector) Helmholtz equation just happens to be awkward numerically, due to the fact that when it is written in the form $Ax = b$ (cf. the discussion preceding eq (3.5)) the matrix A is not positive definite, even when full information is given on the boundaries. How to overcome this difficulty is the subject of current research (see e.g. [26] and references therein), and in the summary we shall comment upon possible future improvements on our scheme. For the present examples we use the truncated SOR method.

3.2 Two-Dimensional Examples

In this subsection we present two-dimensional examples which were used to develop the procedure and test dependence on various parameters. All the examples assume a cavity of rectangular cross section with perfectly conducting walls with dimensions a×b×c. The $TE_{\ell mn}$ mode of the cavity is given by

$$\begin{aligned} A_x &= \cos\frac{\ell\pi x}{a}\ \sin\frac{m\pi y}{b}\ \sin\frac{n\pi z}{c}\ , \\ A_y &= -\frac{\ell b}{ma}\ \sin\frac{\ell\pi x}{a}\ \cos\frac{m\pi y}{b}\ \sin\frac{n\pi z}{c}\ , \\ A_z &= 0, \end{aligned} \tag{3.10}$$

where we have chosen unit amplitude and assumed $m \neq 0$. The dimensions will always be chosen to correspond to resonance of the mode used to specify "measurement" results, $(\ell/a)^2 + (m/b)^2 + (n/c)^2 = 4$. This is necessary in order to have any solution at all in the enclosed cavity in the absence of any source. In these preliminary examples we restrict ourselves to cases where only one component (A_x) of the vector potential is nonzero, and then in order to restrict the problem to two dimensions we impose constancy of A_x in the x direction. The divergence condition (3.2a) is then automatically satisfied, and we need only treat the Helmholtz equation (3.2b).

In the first computation we assume the field is measured at one point, the center of the cavity, where $A_x = 1.0$, $A_y = A_z = 0$. The cavity dimensions are taken to be $a = 2b = 2c = \sqrt{2}$, which corresponds to the resonant frequency for the TE_{011} mode. The tangential components of $\vec{A}$ are fixed at zero ateach wall, and A_x is required to be constant in x. The relaxation method outlined above is used, and the iteration process is terminated when the magnitude of the A_x residual averaged over the volume, $\langle|R_x|\rangle$, reaches a minimum. This first example is atypical in that $\langle|R_x|\rangle$ decreases asymptotically to a constant, and so our solution is the field configuration any time after $\langle|R_x|\rangle$ has reached its limit value, which is about 0.4×10^{-4}. A value of $\Omega_H \simeq 1.75$ resulted in the fastest convergence to the limit.

The y dependence of A_x for two different values of z and two different grid sizes is shown in fig. 3-1. The solid and dashed curves represent the field configuration for the TE_{011} mode, which is the only mode resonant at this frequency which is consistent with the measurement. It is evident that the 16×8×8 grid is sufficiently fine for our purposes. The z dependence of A_x for fixed y is virtually identical to the y dependence for fixed z and

therefore is not shown. The final results for A_y and A_z are zero everywhere, as they should be.

At the beginning of the computation, initial values of the field at all points must be assigned. Two different starting configurations were tried. In one, $\vec{A}$ is initially zero at all points except measurement points,where of course it assumes the measured values. In the other, a smooth initial configuration is generated by an algorithm which interpolates between measurement points and boundary points. For this example, the same results are obtained for either initial configuration. In general the smooth initial configuration tends to yield a lower minimum $\langle|R_x|\rangle$, and we shall use it in the following examples unless otherwise noted. We expect that when multiple solutions exist the smooth starting configuration will result in the smoothest of the possible solutions. This should correspond to the lowest mode.

If the measurement point is moved from the center in this TE_{011} example, the quality of the solution deteriorates. For example, if the measurement is made at (y,z) = (b/4, c/2) then the computed solution at the center is about 6% higher than the correct solution, as shown in fig. 3-2.

Turning to a more complex field configuration, we consider the case of four measurements with A_x = 1.0 at (b/4, c/4) and (3b/4, 3c/4) and A_x = -1.0 at (3b/4, c/4) and (b/4, 3c/4). The lowest mode consistent with those values is the TE_{022} mode, and we choose a=b=c= $\sqrt{2}$ so that it is resonant. In this case we encounter what proves to be the typical behavior of $\langle|R_x|\rangle$. It decreases with successive iterations at first, but it levels off, begins to increase, and eventually blows up. The value Ω_H = 1.75 again results in the quickest minimum, and other values of Ω_H do not result in a significantly better solution. We use as our approximate solution the field configuration for which $\langle|R_x|\rangle$ is a minimum with Ω_H = 1.75. The results of figure 3-3 then

follow. The solid and dashed curves represent the TE_{022} mode, and again the agreement is very good. The same is true for the z dependence, which is not shown.

Equally good results were obtained using four measurements representing the TE_{021} mode, using a cavity with dimensions a=b=2c = $\sqrt{2}$. The measurement points were taken to be the same as in the TE_{022} case above, with the measured values different of course. Figure 3-4a compares the computed A_X to the TE_{021} form as a function of y at z=c/2, and fig. 3-4b does the same as a function of z for y=b/4. A 16 × 16 × 8 grid was used, with Ω_H = 1.75

The results thus far have been very encouraging. Instructive difficulties arise when a=b=c= $\sqrt{0.8}$, however. If we use as measurements the TE_{021} field at two points, (y,z) = (b/4, c/2) and (3b/4, c/2), the agreement of the computed results with the TE_{021} field shape is not satisfactory. This is demonstrated in fig. 3-5. In this and succeeding examples, the largest dimension is divided into 16 divisions, with other dimensions divided proportionately. Thus, this grid is 16x16x16. Away from the measurement points the computed field falls off too rapidly. The problem persists when the number of measurement points is increased to four, as is evident from fig. 3-6. The value of the minimum $\langle|R_X|\rangle$ is somewhat larger than the TE_{022} and rectangular TE_{021} cases: 0.25×10^{-2} as opposed to 0.20×10^{-2} and 0.11×10^{-2} respectively.

It is not completely clear what cause underlies these difficulties. The numerical method being used does not actually converge to the true solution; it approaches it and then wanders off, with the approximate solution being obtained by taking the fields when "closest" to the true solution (as determined by $\langle|R_X|\rangle$). In the present case (TE_{021} with square cavity cross section), the iterative process just does not get that close to the correct

result. The most likely reason appears to be that there are two possible resonant modes with $A_y = A_z = 0$ at this frequency, TE_{021} and TE_{012}, and the computation does not pick out one pure mode.

3.3 Three-Dimensional Examples

We now allow variation in the x direction and treat the fully three-dimensional case. This requires simultaneous solution of both the vector Helmholtz equation (3.3b) and the divergence condition (3.3a). Again we start with the simplest possible field configuration, assigning values corresponding to the TE_{011} mode at measurement points. Six measurement points were used, located at (a/8, b/8, 7c/8), (a/4, 7b/8, c/4), (3a/8, b/2, c/2), (5a/8, 3b/4, 3c/4), (3a/4, b/4, c/4), and (7a/8, 7b/8, 7c/8). The points are scattered irregularly to cover the entire volume and to avoid having them all at zeros of some low order mode. The box dimensions are taken to be $2a=b=c=1/\sqrt{2}$, and an 8×16×16 grid is used.

The computation proceeds in much the same manner as the preceding ones, except that now the grid has three instead of two dimensions, and the divergence condition relaxation (3.9) is also performed at each point. The quality of the solution depends on the choice of the relaxation parameters, Ω_H and Ω_∇. The minimum value of $<|\vec{R}_H|>$ decreases as Ω_H increases, but very slowly, whereas the minimum value of $<|R_\nabla|>$ is smallest for small Ω_H and increases rather rapidly as Ω_H increases. The minima of both residuals are smallest when Ω_∇ is large. The optimal choices seem to be around $\Omega_H = 0.2$, $\Omega_\nabla = 1.75$, which are the values we used. Representative results of the computation are shown in fig. 3-7. The y dependence is satisfactory, but only satisfactory, and a similar comment applies to the z dependence (not shown). For the most part, the x dependence is very good--the computed A_x is very

nearly flat. The one exception occurs along the line through the center of the yz plane. Significant deviations from constancy occur, particularly at the measurement point x/a = 3/8 where A_x is constrained to be 1.

The TE_{011} results are not bad in themselves, but they do not bode well for more complicated cases, which will have greater spatial variation and more than one nonzero component of $\vec{A}$. The forebodings are borne out when we usemeasurement results corresponding to the TE_{022} mode. With six measurement points we were unable to obtain acceptable results. In fact for some values of Ω_H and Ω_∇ the average residuals $\langle|\vec{R}_H|\rangle$ and $\langle|R_\nabla|\rangle$ increased steadily from the start of the computation--the best field configuration was the initial guess. Increasing the number of measurement points to eleven did not improve matters significantly. Also, the difficulties persisted when we used different indicators of solution quality, such as max(R) or $\langle R\rangle$.

We conclude that in general three-dimensional problems, given just a few measurement points, solving the Helmholtz equation and divergence condition using the truncated SOR method fails to obtain useful approximate solutions. To investigate whether the numerical method is more successful when the field is specified at a large number of points, we did computations with all components of the field fixed at all boundary points. The boundary points are chosen because they can be thought of as driving the solution; when the field is known at all boundary points there is a unique solution. We wish to investigate whether our truncated SOR method can obtain something like the correct solution and, if so, whether it can do so when some of the boundary points are not given.

We have obtained results for a number of low order modes. A good example is the TE_{123} mode, which was the highest mode considered. For convenience, a composite residual was defined by

$$R(\alpha) \equiv \alpha \langle|\vec{R}_H|\rangle + (1 - \alpha)\langle|R_\nabla|\rangle, \tag{3.11}$$

and the solution was chosen as the point at which $R(\alpha)$ was a minimum. A number of values of α were used, and the results were relatively insensitive to the exact value. In the computations we used $\alpha = 0.5$. Figure 3-8 compares the computed A_x and A_y (A_z is zero) to the correct TE_{123} results as functions of y at x = a/4 and z = c/8 and c/2. The agreement for A_x is seen to be very good in both cases, but the A_y results fail to reproduce the extremum at the center. In order to check that this is not due to some programming clumsiness which introduced a spurious asymmetry in the treatment of A_x and A_y, we also computed the TE_{213} mode with dimensions a and b interchanged. We found that the A_x and A_y results were also just interchanged, as should be the case. The difficulties apparent in fig. 3-8 can therefore be taken as indications of deficiencies in the truncated SOR method rather than the consequence of (obvious) programming blunders. The poor results at central y will also be reflected in the x and z dependence at fixed y. This is seen in figure 3-9, where the (x,y) = (a/4, b/8) results are very good but the (a/2, b/2) result is less than half the correct answer.

The TE_{123} mode constitutes a rather demanding test. There is different spatial variation in each of the three directions, two components are nonzero, and the components have different spatial dependence. The numerical solutions are quite good over most (~7/8) of the volume but fail in the central region. A finer grid led to only slight improvement. When the fields are completely specified on the boundary, this truncated SOR method could be useful in generating a starting configuration for some other method which converges (as it was used in [26]), but it does not produce satisfactory results by itself.

Finally, if the fields are specified only at one-fourth of the boundary points (tangential fields still vanishing at all boundary points), no minimum of R is obtained for the TE_{123} mode. From the start of the computation each iteration increases R. In principle we could fix unmeasured boundary points by interpolation and might then obtain a minimum for R, but at this time that appears to be beating a dead horse.

4. DISCUSSION AND CONCLUSIONS

We have suggested an approach to the characterization of EM environments which is based on the numerical solution of Maxwell's equations subject to the constraints imposed by boundary conditions and results of measurements of the field at a relatively small number of points. Some success was achieved in the simpler examples used to demonstrate the approach, but results in more complicated three-dimensional examples were less impressive. The comparisons made were of the field configurations, which constitute a far more demanding test than does a global quantity such as the average power density. The results of a less stringent test could well be less disappointing. Nevertheless, it is clear that the method is not yet ready for real applications. The basic obstacle to practical use of the approach is the lack of a fully successful method for obtaining numerical solutions of Maxwell's equations under these conditions.

Two different numerical techniques were investigated. The one based on the action functional and Hamilton's principle founders due to our inability to numerically locate a stationary point which is not an extremum. Having previously tried a Gauss-Seidel type of procedure [21,22] and having found it lacking, we performed an analytic continuation to imaginary time. This has the advantage that the action then has a minimum. Furthermore, the solution

obtained is that with the minimum energy density consistent with the measurements. This technique, however, proved to be inapplicable to cases in which there was any spatial variation of the phase or any phase difference between different components of the field. We therefore abandoned the attempt to develop a numerical technique based on the stationarity of the action. If one did insist on pursuing this line further, one possibility would be to construct and numerically minimize the function defined by

$$D^2 \equiv \sum_{i,j,k} \left[\left(\frac{\partial a}{\partial A_x(i,j,k)} \right)^2 + \left(\frac{\partial a}{\partial A_y(i,j,k)} \right)^2 + \left(\frac{\partial a}{\partial A_z(i,j,k)} \right)^2 \right] . \qquad (4.1)$$

D^2 is a nonnegative function whose zeros correspond to stationary points of the action and therefore to solutions of Maxwell's equations. Obvious problems with that tactic are that the construction of D^2 is quite awkward and that there is no guarantee that it can be easily minimized.

The second technique we studied in detail was use of successive over-relaxation (SOR) to simultaneously solve the vector Helmholtz equation and the divergence condition, which are equivalent to Maxwell's equations in the cases considered (sourceless, free space, one frequency). Since the SOR method does not converge for the Helmholtz equation, the sequence of iterations was truncated when the volume average of the magnitude of the residual was a minimum. This produced good results in a number of cases but failed in others. Even when the field was completely specified on the boundary, the results were not always satisfactory.

There are various other possible numerical procedures which come to mind. Mittra and coworkers at Illinois have had some success using a modified Gauss-Seidel method on problems of the form $Ax = b$ where A is not positive definite. The modification they make is to introduce a convergence factor which prevents

the Gauss-Seidel iterations from diverging [27]. This is similar to our truncated SOR method, with the truncation replaced by a gradual damping (and with $\Omega = 1$). It does not appear likely that the gradual damping would cure the ills of the truncation method. The divergence problem is obviated by the truncation method too. The difficulty is that the iterative procedure does not approach very close to the correct solution in some cases, and the introduction of a convergence factor does not address that problem.

A more promising alternative would be to try a truncated conjugate gradient procedure, as has been used in ill-conditioned deconvolution problems [28]. Some work would be required to adapt the procedure to our case, in particular to develop a criterion for when to truncate the iterations. If the method can be applied, it could prove very useful since proponents of the procedure claim it yields a minimum-norm solution. For our problem that corresponds to the minimum energy density solution.

One seemingly relevant method which proves inapplicable is the maximum entropy method (MEM), as reviewed for example in [29]. It is highly effective for reconstructing images which have been blurred, contaminated by noise, or from which some fraction of the information is missing. Our problem falls into the missing information category. Unfortunately, for the MEM to work it requires several pieces of information per unit cell, where the cell size corresponds to the volume over which the information at a point has been smeared. Since there is no blurring in our problem there is no information except at the measurement points, and the MEM is powerless to fill in the empty space.

A final possibility we mention is to put the Helmholtz equation in the form $Ax = b$, as described in Section 3, and then multiply by the adjoint of A ($A^{\dagger}$) to obtain

$$A^{\dagger} Ax = A^{\dagger}b. \qquad (4.2)$$

If all boundary values are specified the SOR method will converge for this equation since the matrix $A^{\dagger}A$ is then positive definite. Even for incomplete information $A^{\dagger}A$ will not have negative eigenvalues (although some will be zero), and so SOR should be less unstable. As with D^2 of eq (4.1), however, $A^{\dagger}A$ is not so simple to construct. Furthermore, the rate of convergence for iterative solution of eq (4.2) would be expected to be very slow. (This could be improved by using SOR on Ax = b to precondition x.)

In summary, neither of the numerical methods we investigated was successful in all cases. There do exist other methods which may warrant further investigation. The general approach (constrained solution of Maxwell's equations) sounds attractive for characterization of complex environments, but its practical implementation awaits development of better numerical methods.

5. ACKNOWLEDGMENT

We are grateful to John Gary of NBS for a number of patient conversations and helpful comments.

6. REFERENCES

[1] Lerner, E.J. Biological effects of electromagnetic fields. IEEE Spectrum, May 1984, 57.

[2] Beckman, P. Probability in communication engineering. New York, NY: Harcourt, Brace, and World, 1967.

[3] Skomal, E. Man-made radio noise. New York, NY: Van Nostrand Reinhold, 1978.

[4] Middleton, D. Introduction to statistical communication theory. New York, NY: McGraw-Hill, 1960.

[5] Middleton, D. Statistical models of electromagnetic interference, IEEE Trans. EMC-19, no. 3, 106-127, August 1977.

[6] Berry, L. Understanding Middleton's canonical formula for Class-A noise, IEEE Trans. EMC-23, no.4, 337-344, November 1981.

[7] Middleton, D. Canonical and quasi-canonical probability models of Class-A interference, IEEE Trans. EMC-25, no. 2, 76-106, May 1983.

[8] Kanda, M. Time and amplitude statistics for electromagnetic noise in mines, IEEE Trans. EMC-17, no. 3, 122-129, August 1975.

[9] Shepherd, R. Measurements of amplitude probability distributions and power of automobile ignition noise at high frequency, IEEE Trans. VT-23, no. 3, 72-83, August 1974.

[10] Nakai, T.; Kawasaki, Z.I. Automotive noise from a motorway: I, measurements, IEEE Trans. EMC-26, no. 4, 169-174, November 1984.

[11] Nakai, T.; Kawasaki, Z.I. APD's and CRD's for noise from bullet trains in Japan, IEEE Int. Symp. on EMC (Tokyo, Japan), 250-255, October 1984.

[12] Hoffman, H.H.; Cox, D.C. Attenuation of 900 MHz radio waves propagating into a metal building, IEEE Trans. on Antennas and Propagation, Vol. AP-30, No. 4, 808-811, July 1982.

[13] Cox, D.C.; Murray, R.R.; Norris, A.W. Measurements of 800 MHz radio transmission into buildings with metallic walls. The Bell System Technical Journal, Vol. 62, No. 9, 2695-2717; November 1984.

[14] Haskard, M.; Miller, M.; Johnson, A.; Marconi, P. Radio noise measurements in an urban environment, J. Elec. Electron. Eng., Australia, Vol. 2, no. 2, 94-102, June 1982.

[15] Struzak, R.; Rymarowicz, Z.; Moron, W. Urban MF radio noise survey in Poland, Proc. 5th Symp. and Tech. Exhibition on EMC, 1-6, Zurich, 1984.

[16] Parsons, J.; Sheikh, A. Statistical characterization of VHF man-made radio noise, Radio Elec. Eng., Vol. 53, no. 3, 99-106, March 1983.

[17] Randa, J.; Kanda, M. Directional Scanning of complex electromagnetic environments, IEEE Trans. AP-33, no. 12, 1413-1416, December 1985.

[18] Landau, L.D.; Lifshitz, E.M. The classical theory of fields, Chapter 4, Reading, MA: Addison-Wesley, 1962.

[19] Morse, P.M.; Feshbach, H. Methods of theoretical physics, Chapter 3, New York, NY: McGraw-Hill, 1953.

[20] Whittaker, E.T. Treatise on the analytical dynamics of particles and rigid bodies, Chapter 9, New York, NY: Dover, 1944.

[21] Kanda, M.; Randa, J.; Nahman, N.S. Possible estimation methodologies for electromagnetic field distributions in complex environments, NBS Tech. Note 1081, March 1985.

[22] Randa, J.; Kanda, M. A finite-element action approach to the characterization of complex electromagnetic environments, Proc. Int. Symp. on Antennas and Propagation, p. 48-53, Beijing, August 1985.

[23] See, e.g. Itzykson, C; Zuber, J. Quantum field theory. New York, NY: McGraw-Hill, 1980.

[24] Hageman, L.A.; Young, D.M. Applied iterative methods. New York, NY: Academic Press, 1981.

[25] Varga, R.S. Matrix iterative analysis. Englewood Cliffs, NJ: Prentice-Hall, 1962.

[26] Bayliss, A.; Goldstein, C.I.; Turkel, E. An iterative method for the Helmholtz equation, J. Comp. Phys., Vol. 49, 443-457, 1983.

[27] Mittra, R. Electromagnetic Communication Laboratory, Univ. of Illinois, Urbana, IL 61801; private communication.

[28] Sarkar, T.P. et al. Deconvolution of impulse response from time-limited input and output: Theory and experiment, IEEE Trans. IM-34, no. 4, 541-546, December 1985.

[29] Gull, S.F.; Skilling, J. Maximum entropy method in image processing, IEE Preceedings, Vol. 131, Pt. F, No. 6, 646-659, October 1984.

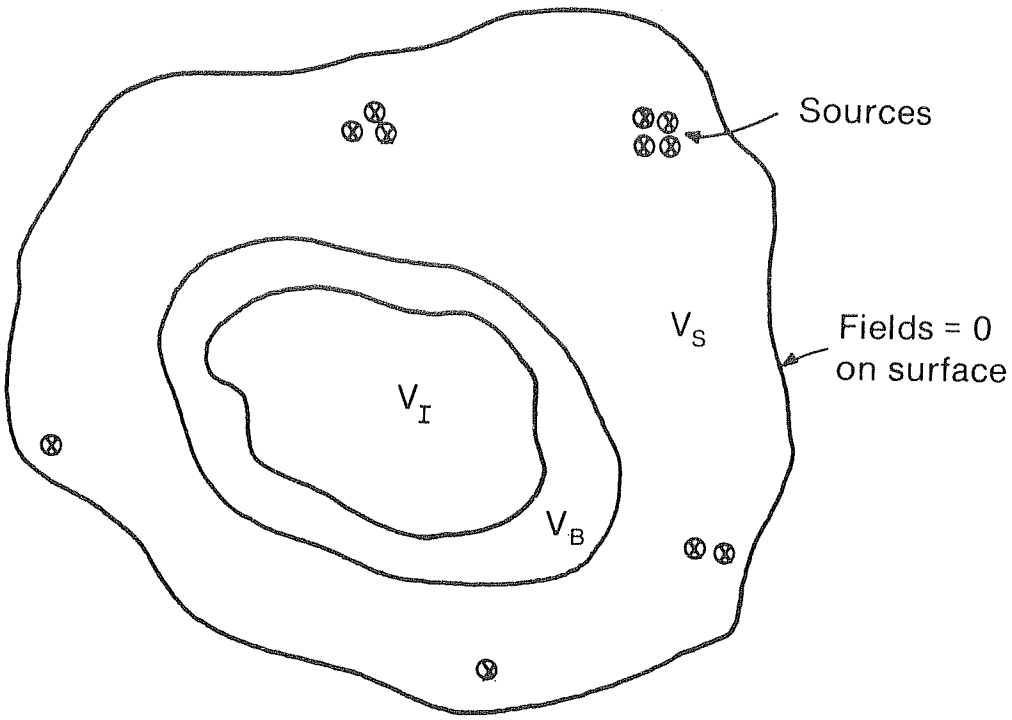

Figure 2-1 Schematic division of total volume into volume of interest (V_I), buffer volume (V_B), and remaining volume containing all sources (V_S).

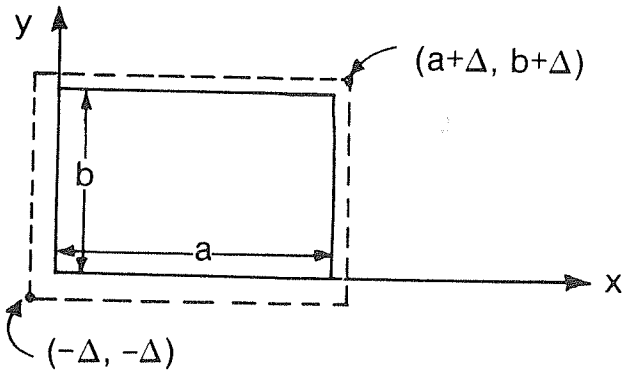

Figure 2-2 Rectangular waveguide dimensions and axes. Also depicted is the boundary of the volume over which the action integral extends.

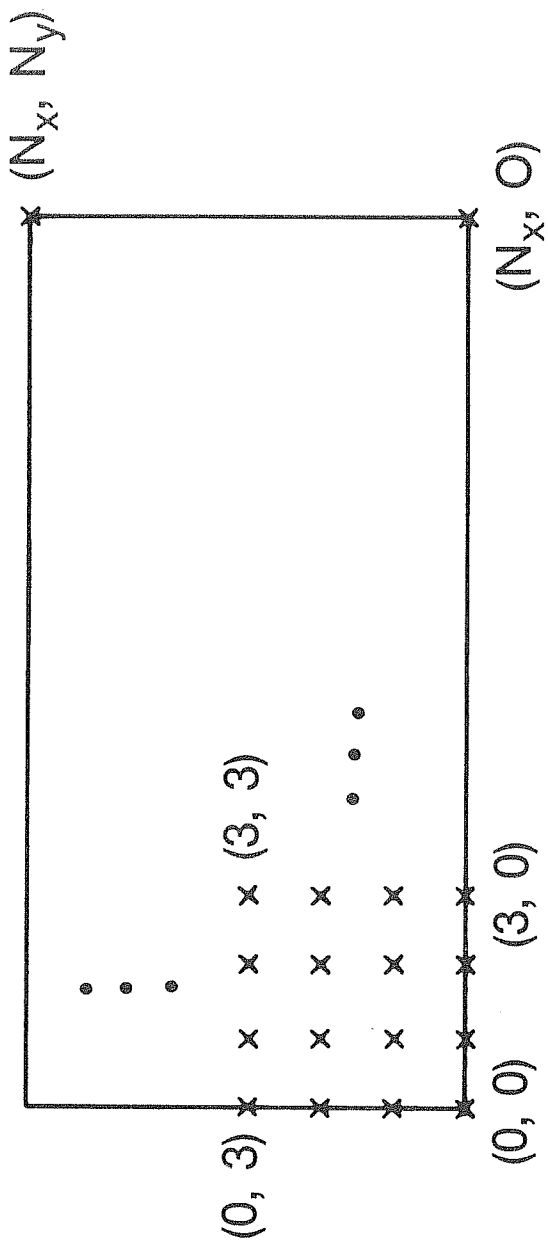

Figure 2-3 Labelling of lattice sties.

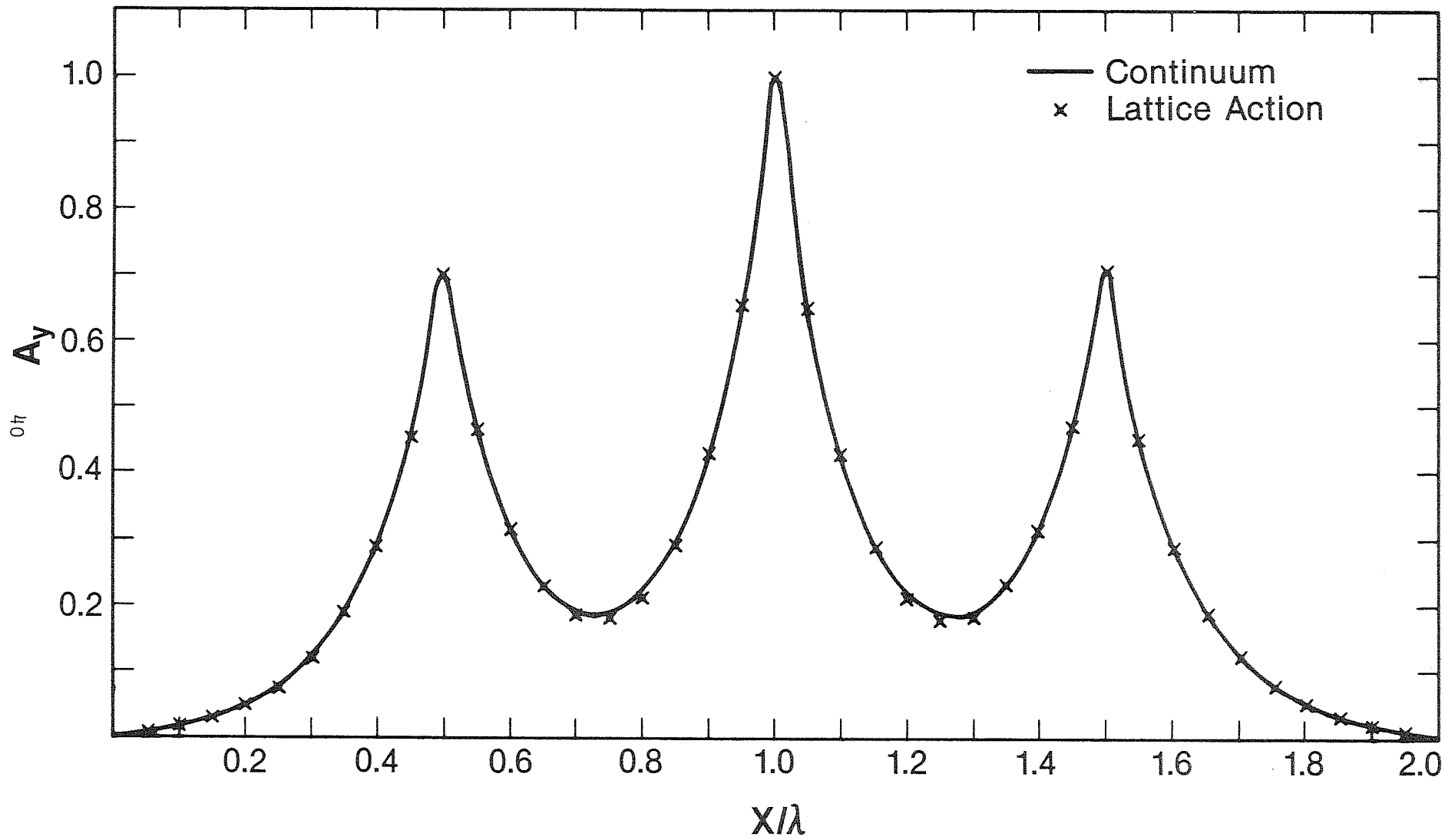

Figure 2-4 Comparison of lattice-action result (crosses) with the continuum result of eqs (2.22,2.28) (solid line) for the one-dimensional case.

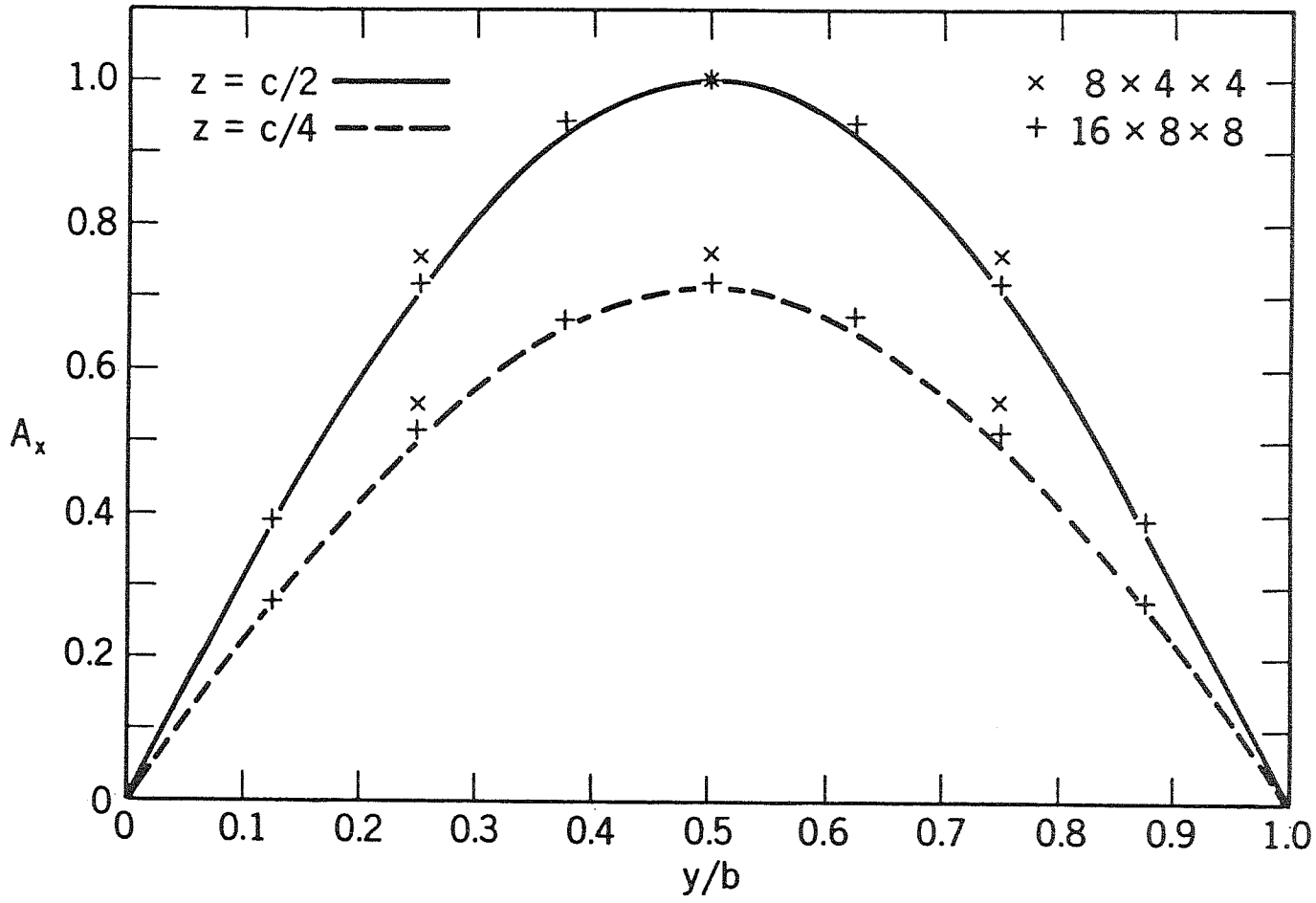

Figure 3-1 Comparison of computed results with TE_{011} field configuration for two different grids. One measurement point was used, located at (a/2, b/2, c/2).

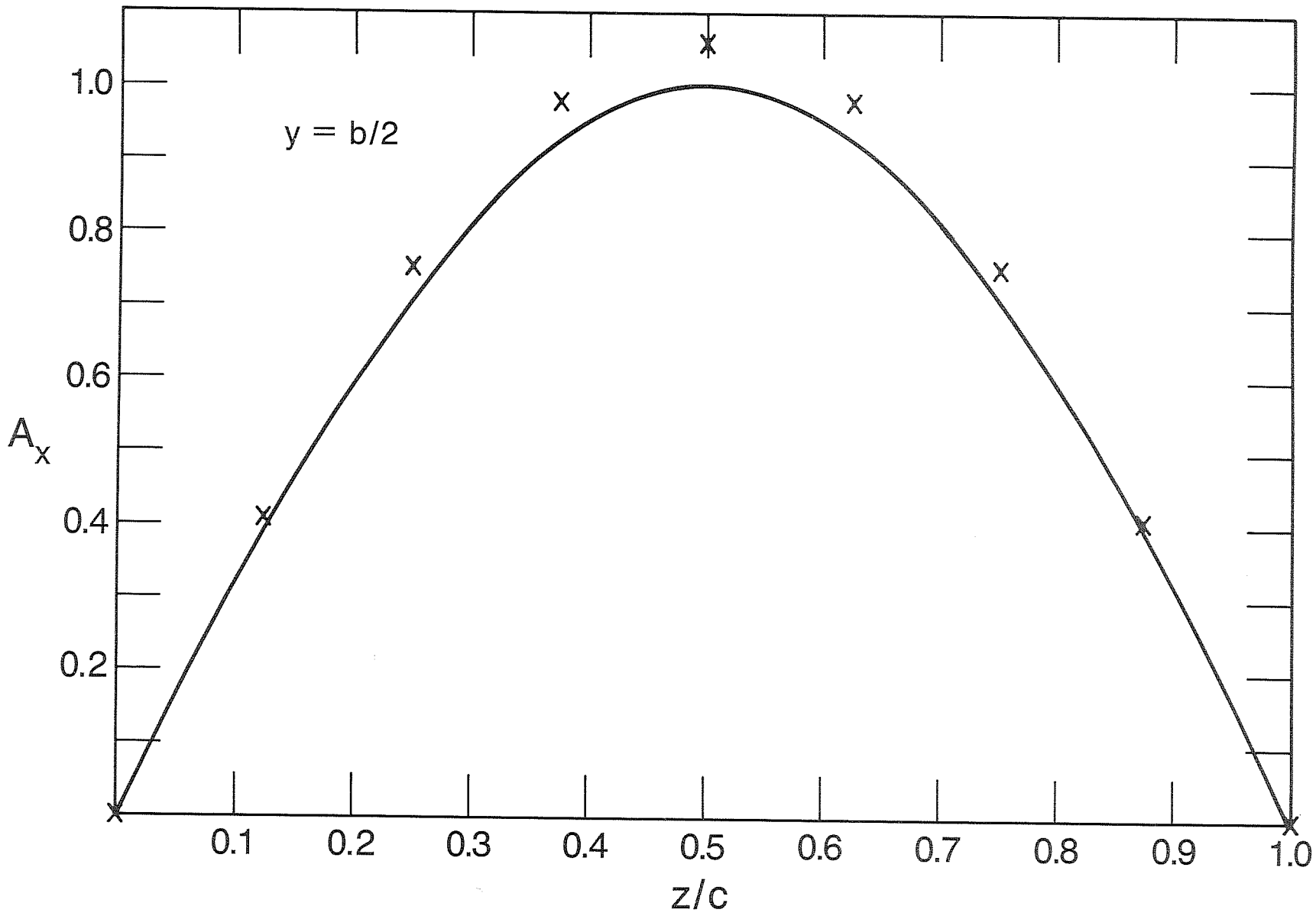

Figure 3-2 Comparison as in fig. 3-1, but with measurement point at (a/2, b/4, c/2). The grid used was 16×8×8.

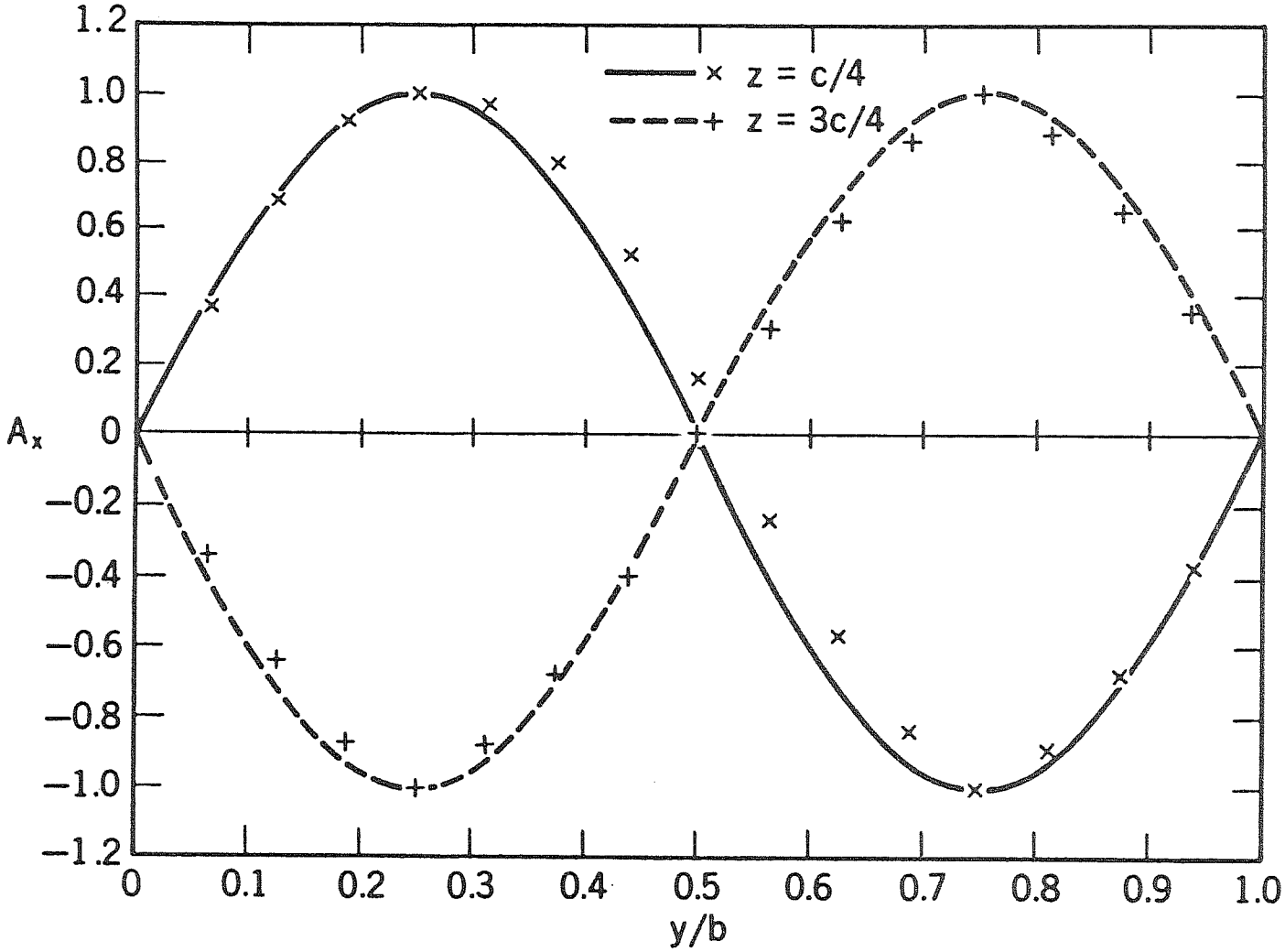

Figure 3-3 a) Comparison of computed results (four measurement points) with TE_{022} field configuration at z = c/4, 3c/4. The grid size was 16×16×16.

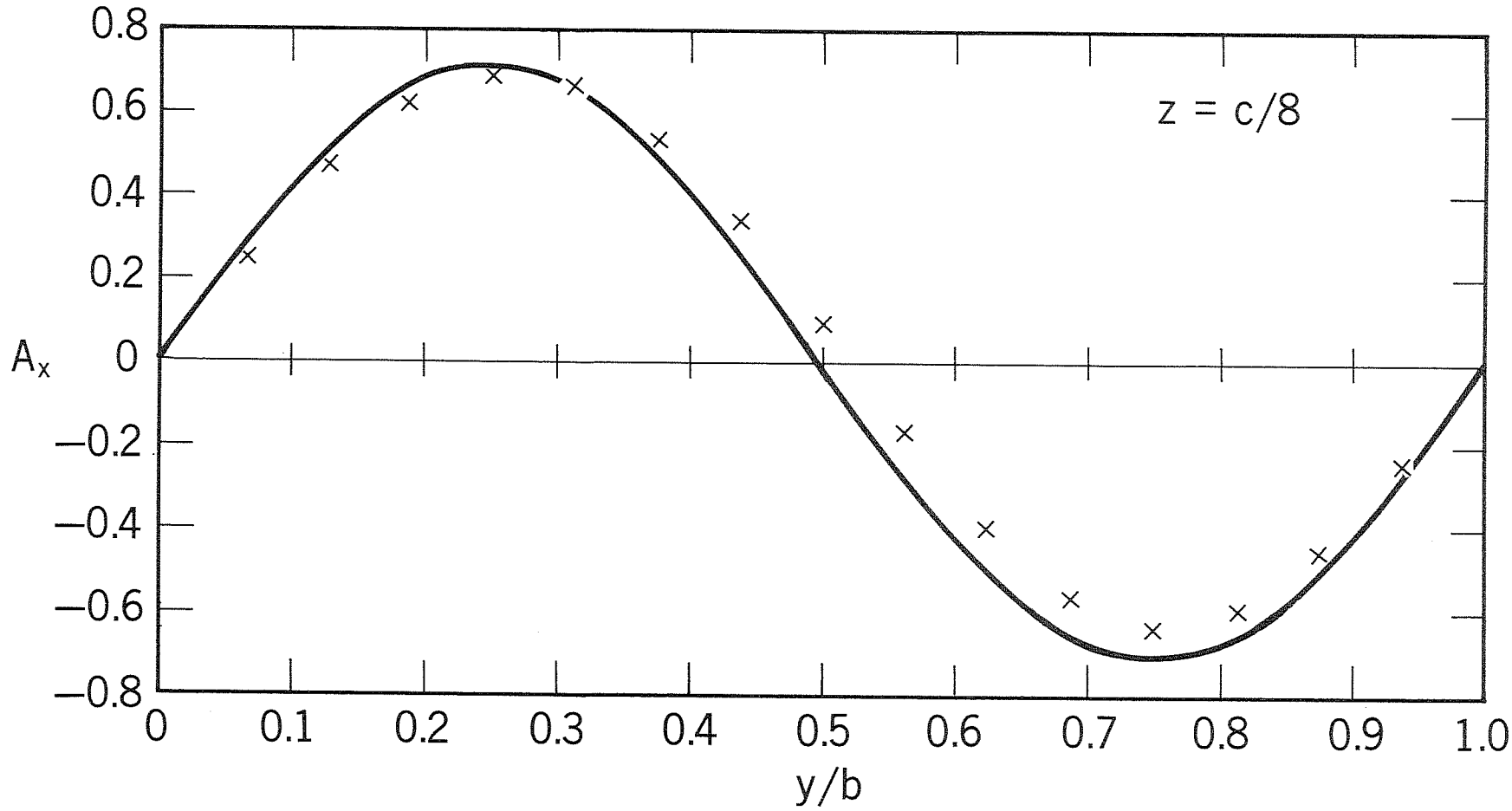

Figure 3-3 b) Comparison of computed results (four measurement points) with TE_{022} field configuration at z = c/8. The grid size was 16×16×16.

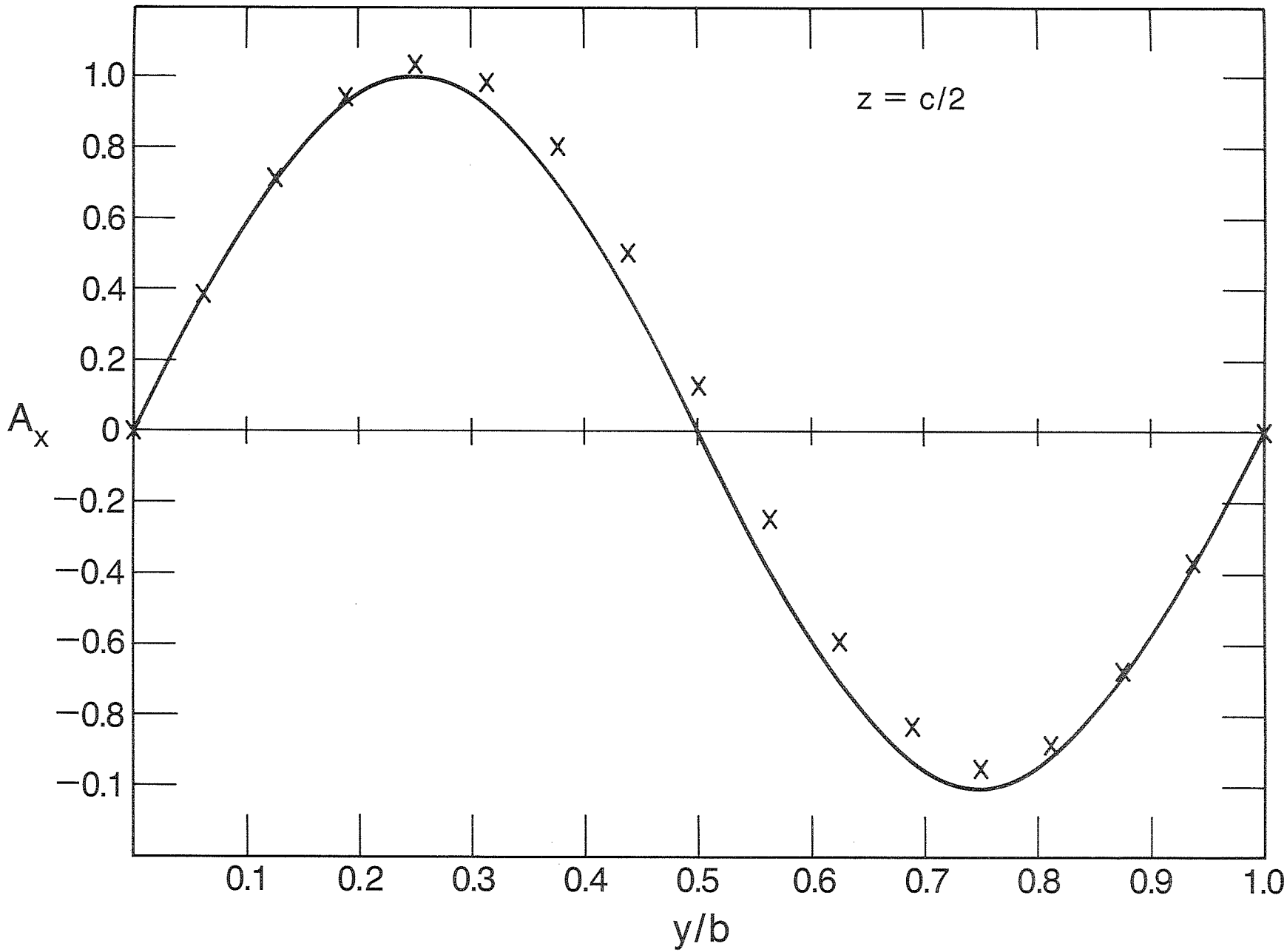

Figure 3-4 a) Comparison of computed results (four measurement points) with TE_{021} field configuration for b = 2c. The grid size was 16×16×8. As function of y at z = c/2.

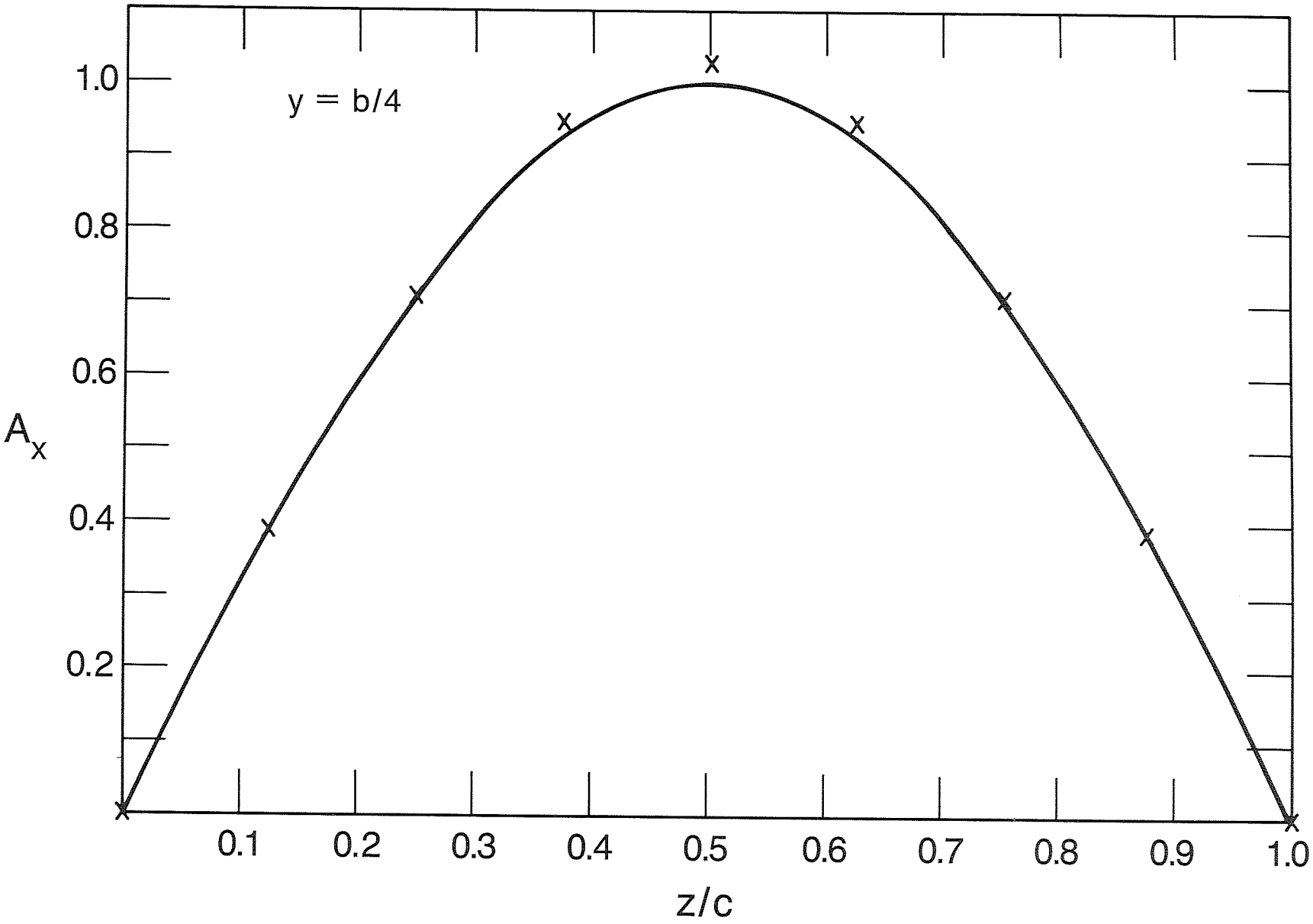

Figure 3-4 b) Comparison of computed results (four measurement points) with TE_{021} field configuration for b = 2c. The grid size was 16×16×8. As function of z at y = b/4.

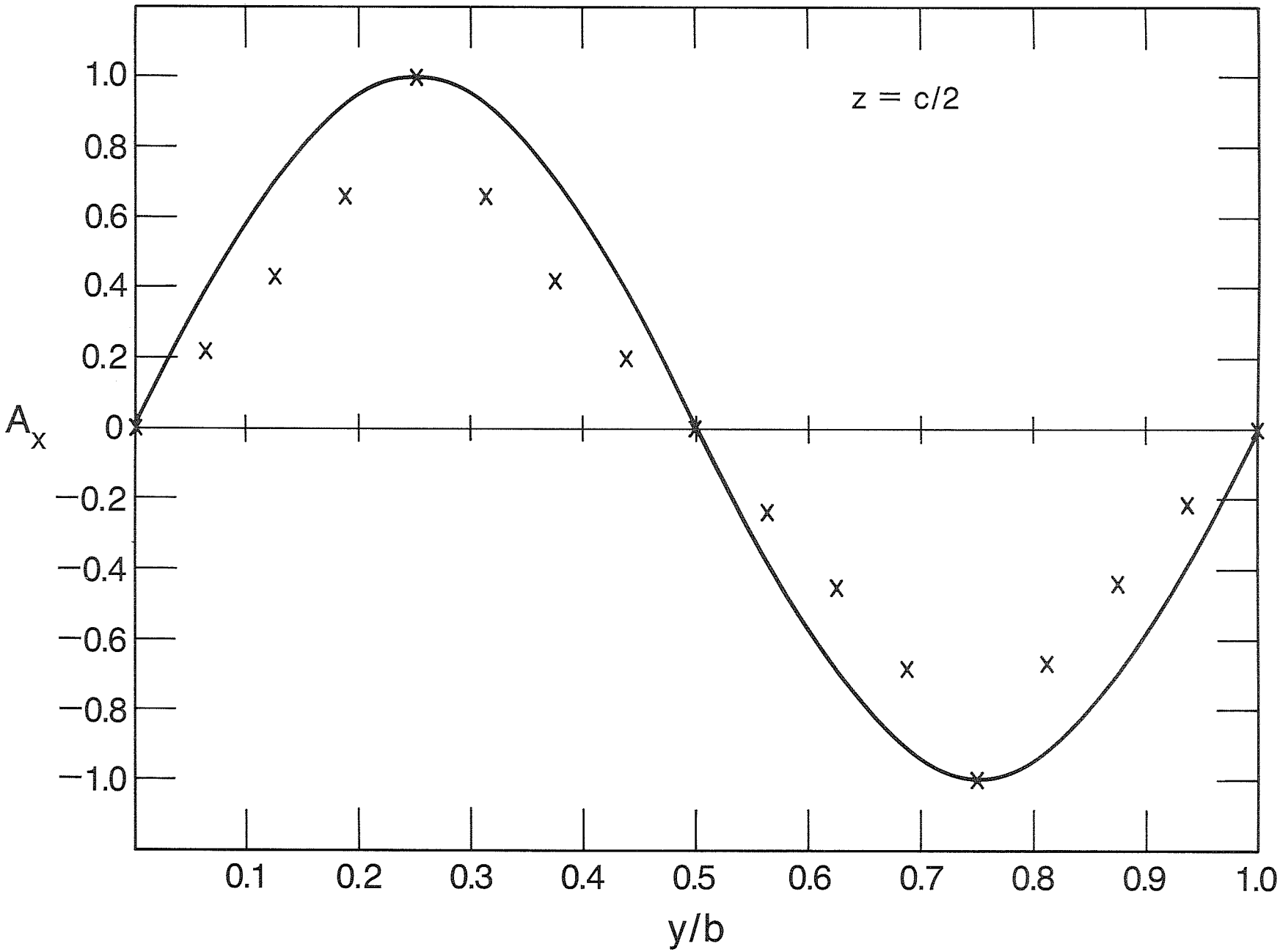

Figure 3-5 a) Comparison of computed results (two measurement points) with TE_{021} field configuration for b=c. As function of y at z = c/2.

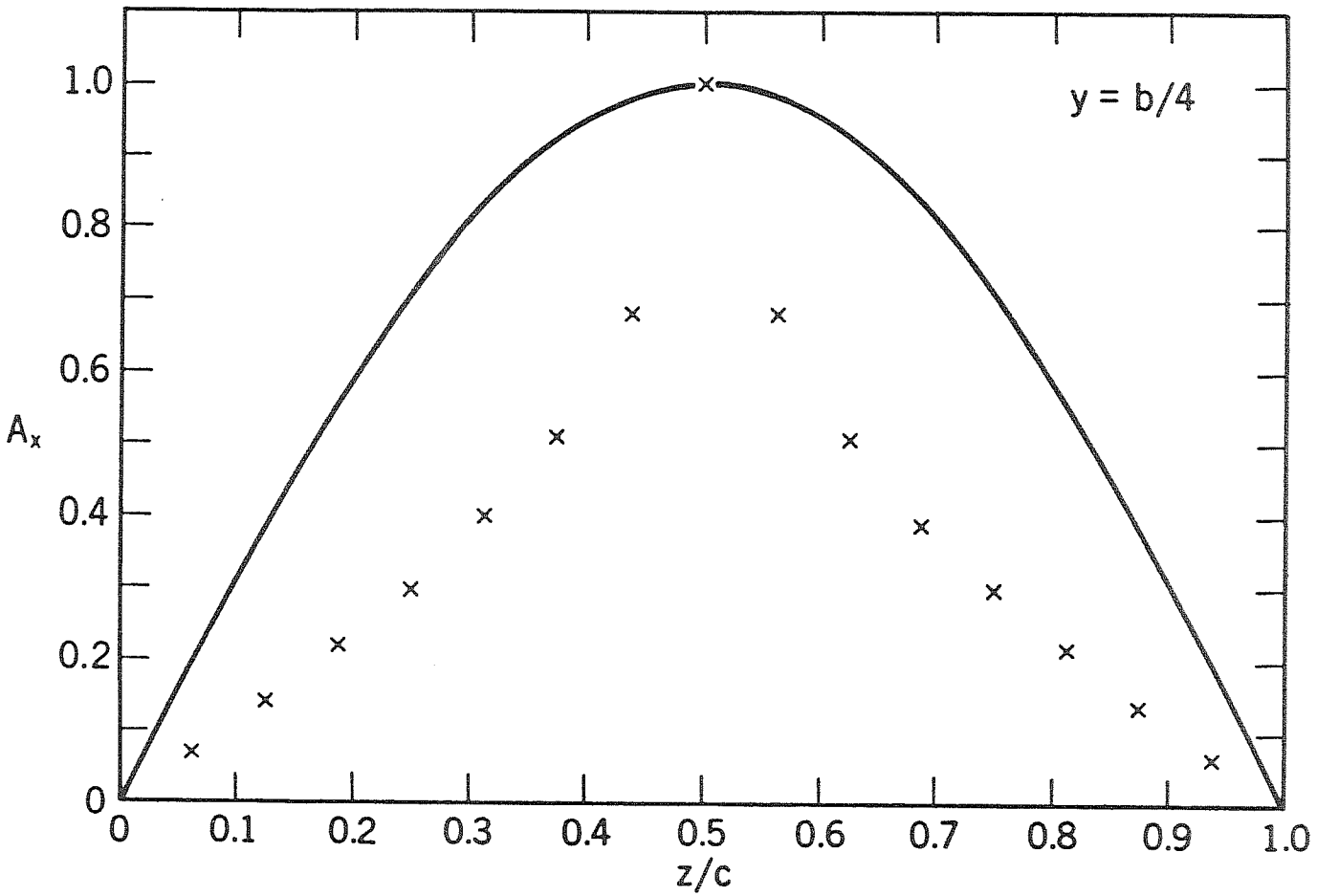

Figure 3-5 b) Comparison of computed results (two measurement points) with TE_{021} field configuration for b=c. As function of z at y = b/4.

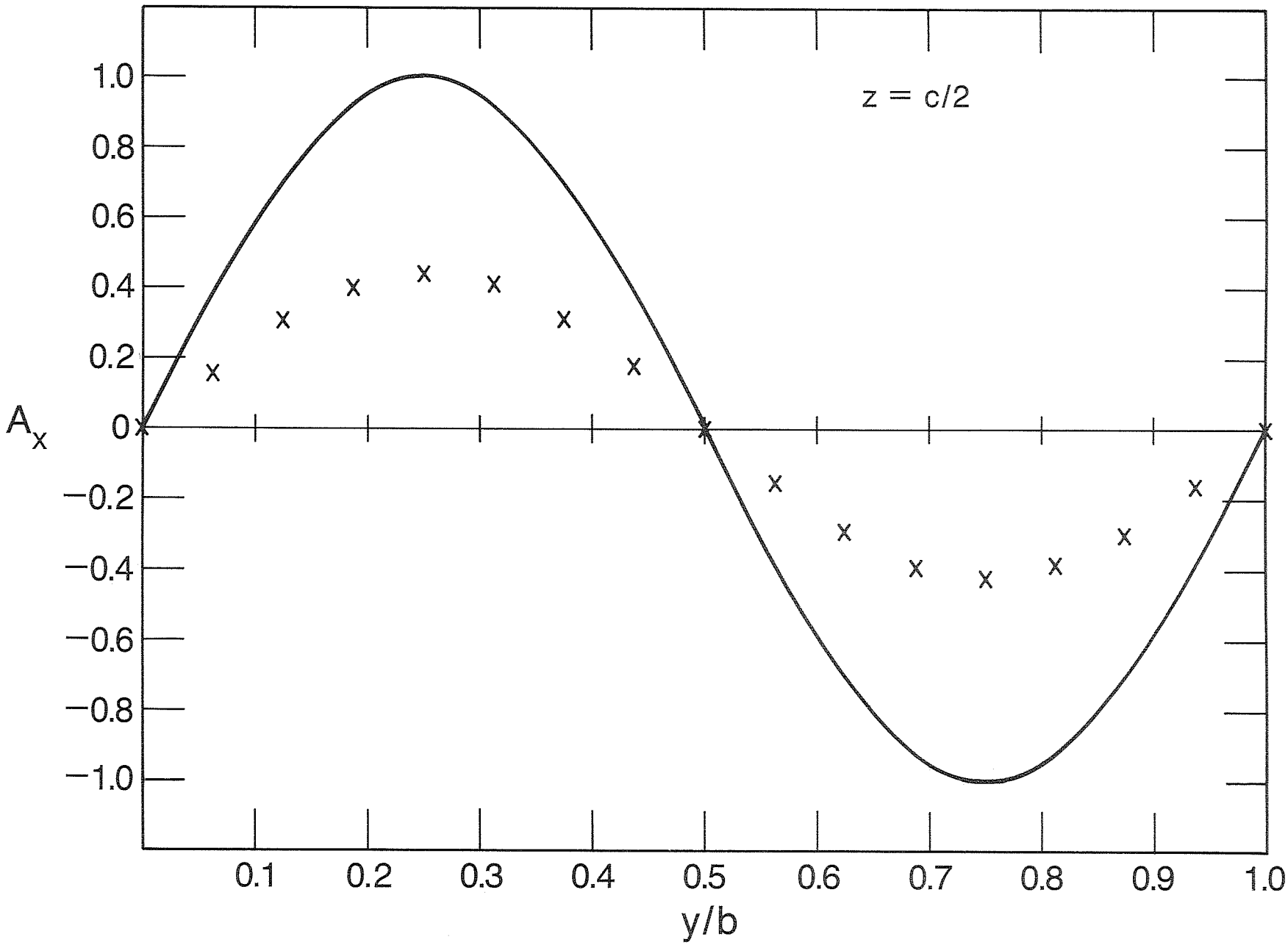

Figure 3-6 a) Comparison as in fig. 3-5 for case of four measurement points, at (y,z) = (b/4, c/4), (b/4, 3c/4), (3b/4, c/4), (3b/4, 3c/4). As function of y at z = c/2.

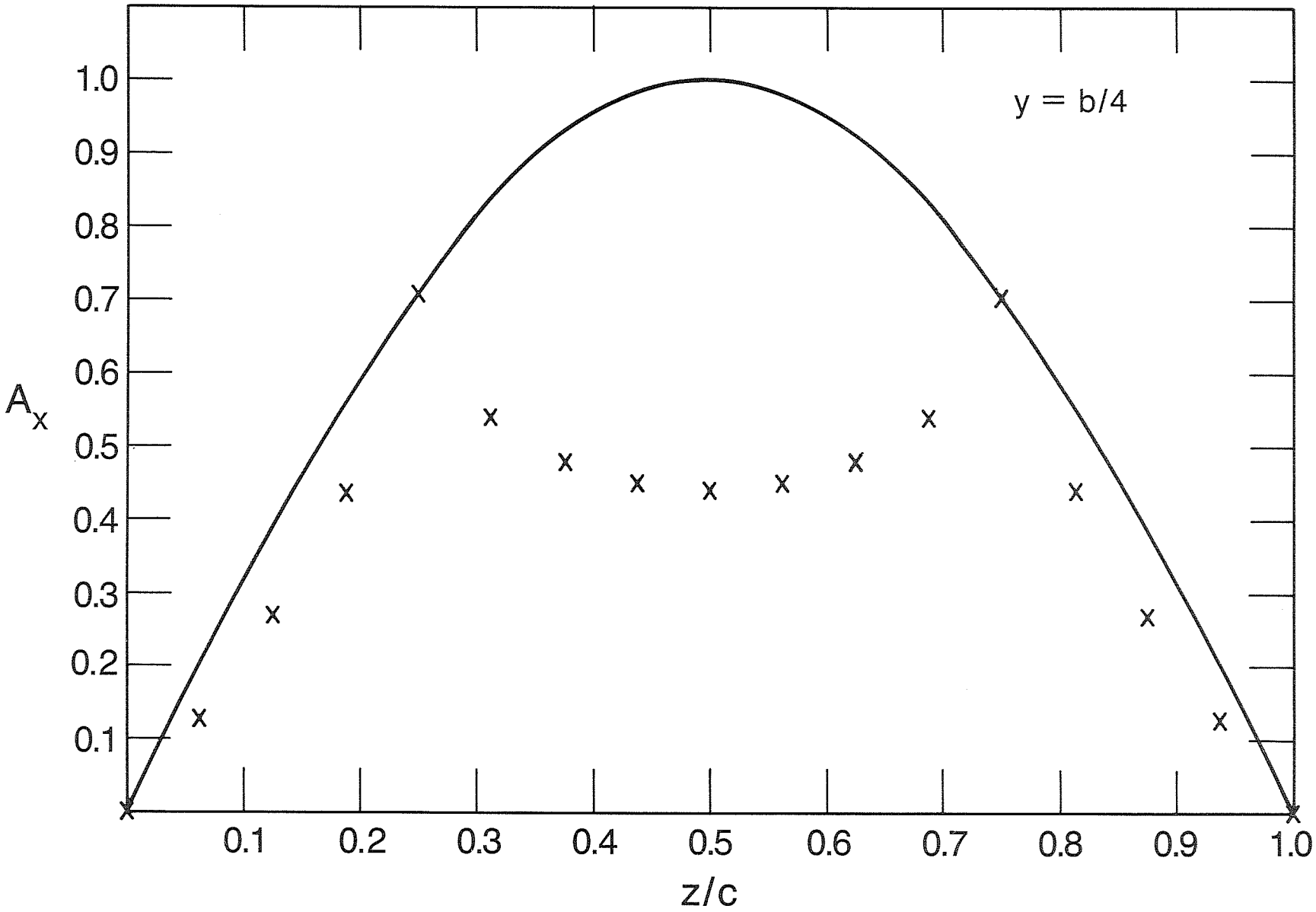

Figure 3-6 b) Comparison as in fig. 3-5 for case of four measurement points, at (y,z) = (b/4, c/4), (b/4, 3c/4), (3b/4, c/4), (3b/4, 3c/4). As function of z at y = b/4.

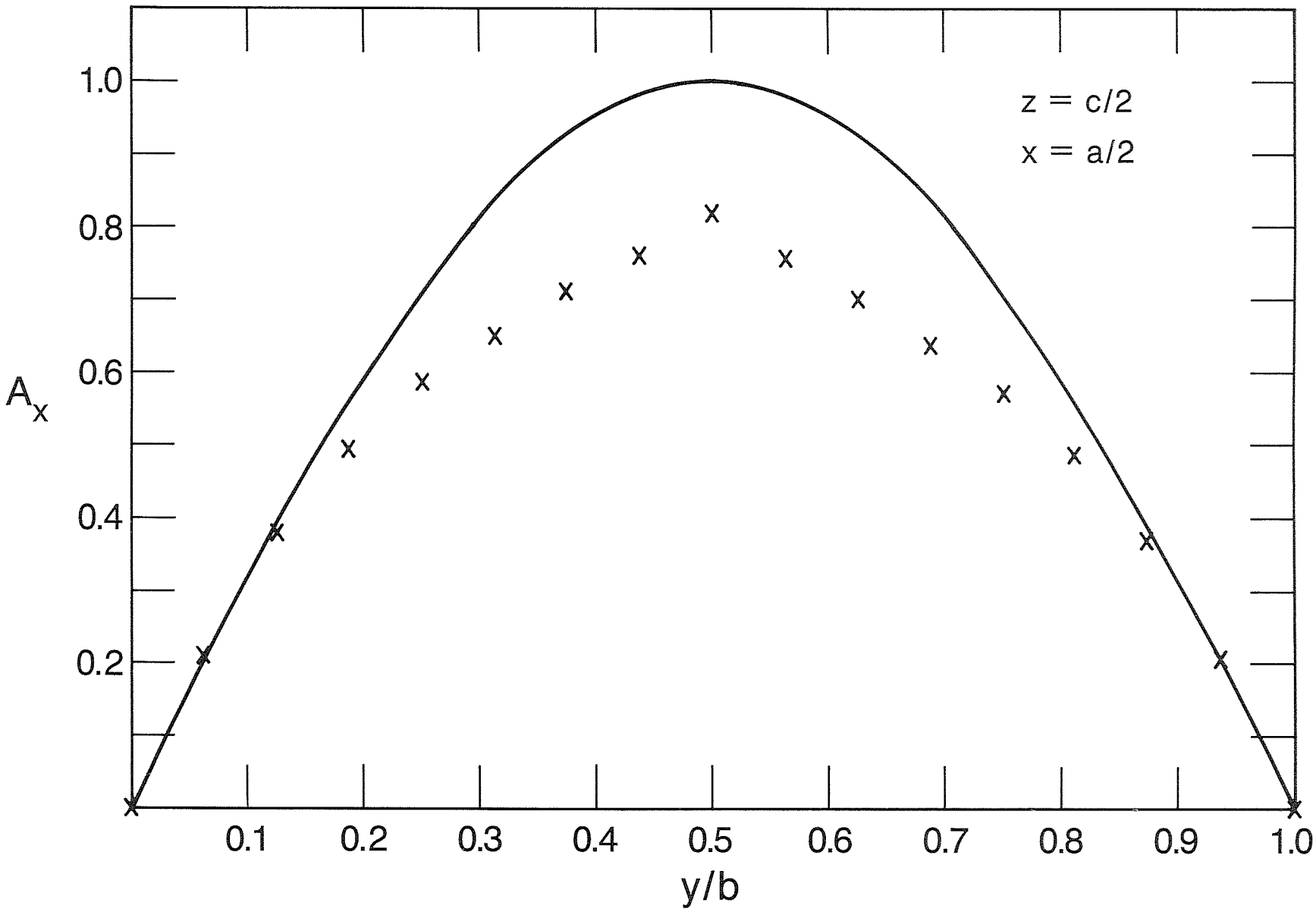

Figure 3-7 a) Comparison of computed results to TE_{011} field for three-dimensional computation. Six measurement points were used. (x,z) = (a/2, c/2).

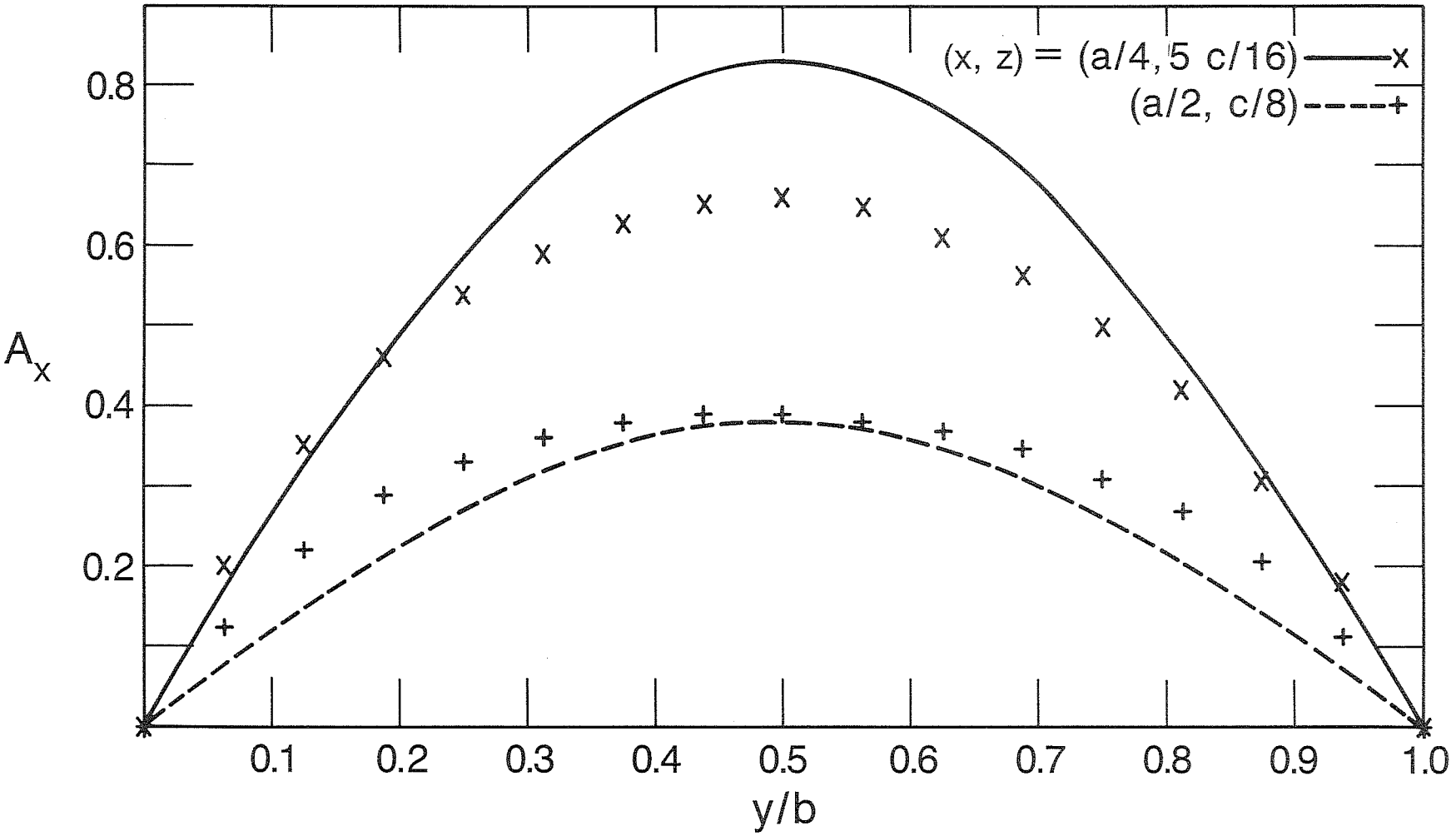

Figure 3-7 b) Comparison of computed results to TE_{011} field for three-dimensional computation. Six measurement points were used. (x,z) = (a/4, 5c/16) and (a/2, c/8).

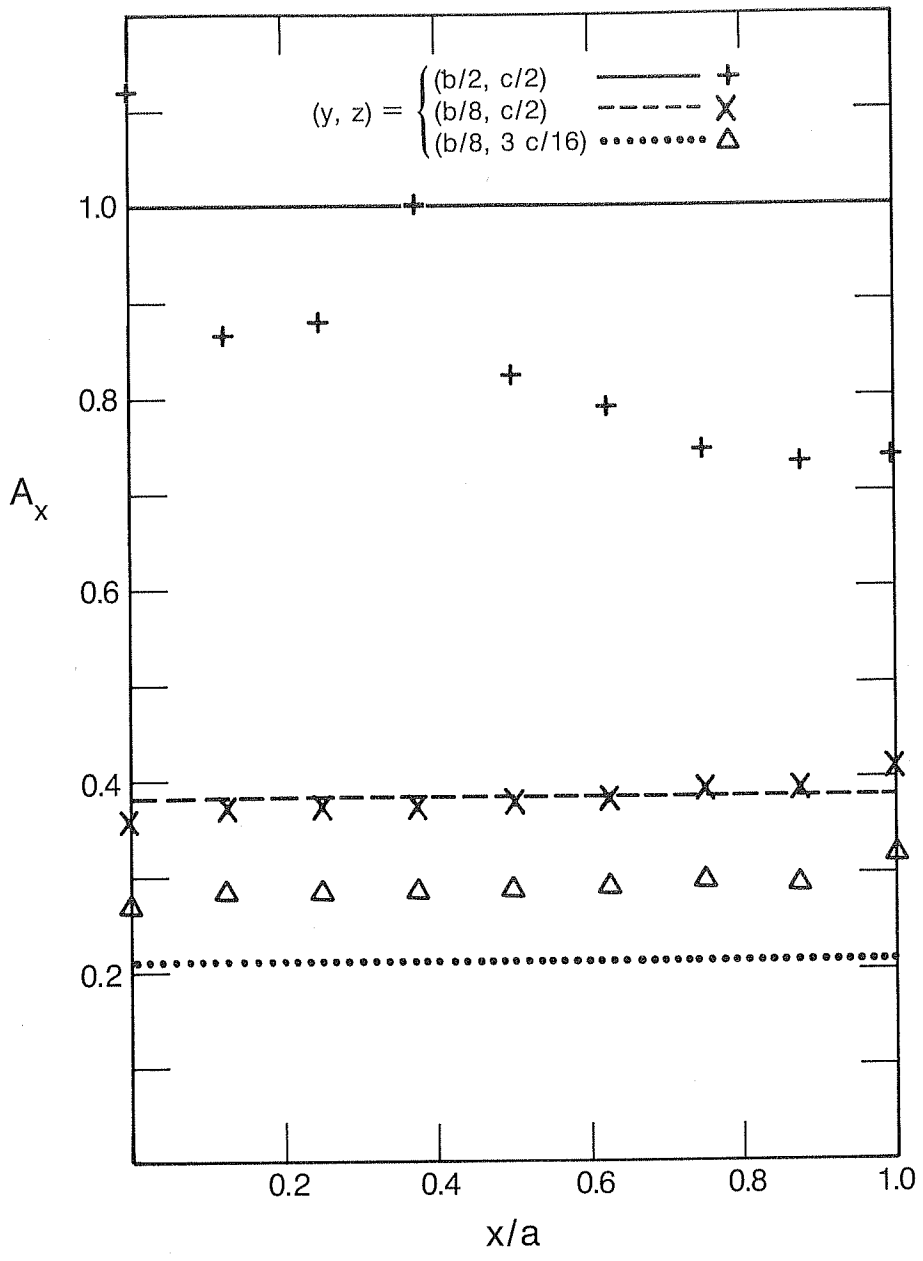

Figure 3-7 c) Comparison of computed results to TE_{011} field for three-dimensional computation. Six measurement points were used. As a function of x for various y and z.

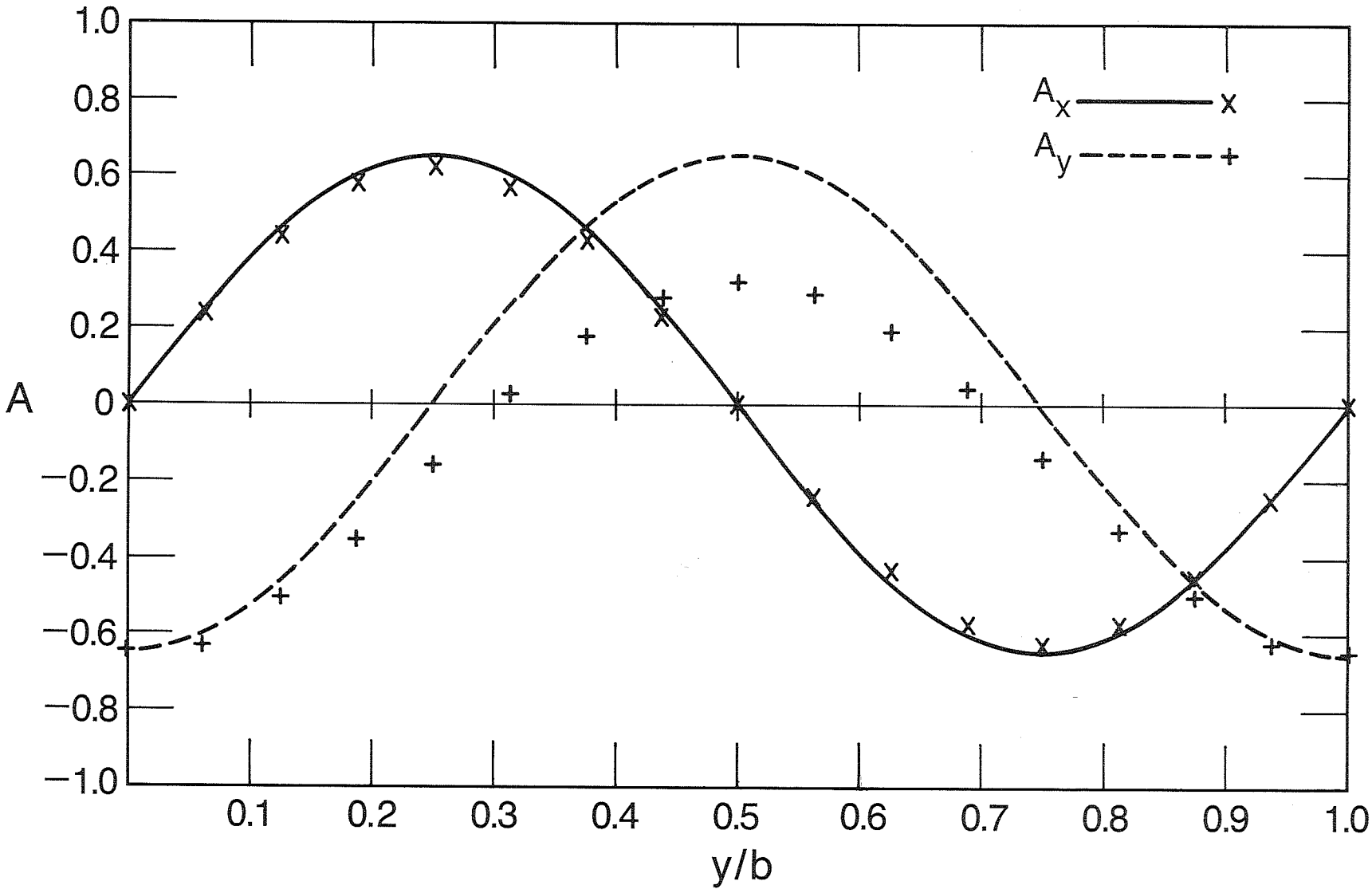

Figure 3-8 a) Comparison of computed results to TE_{123} fields when all components of $\vec{A}$ are fixed on the boundary. As functions of y for (x,z) = (a/4, c/8).

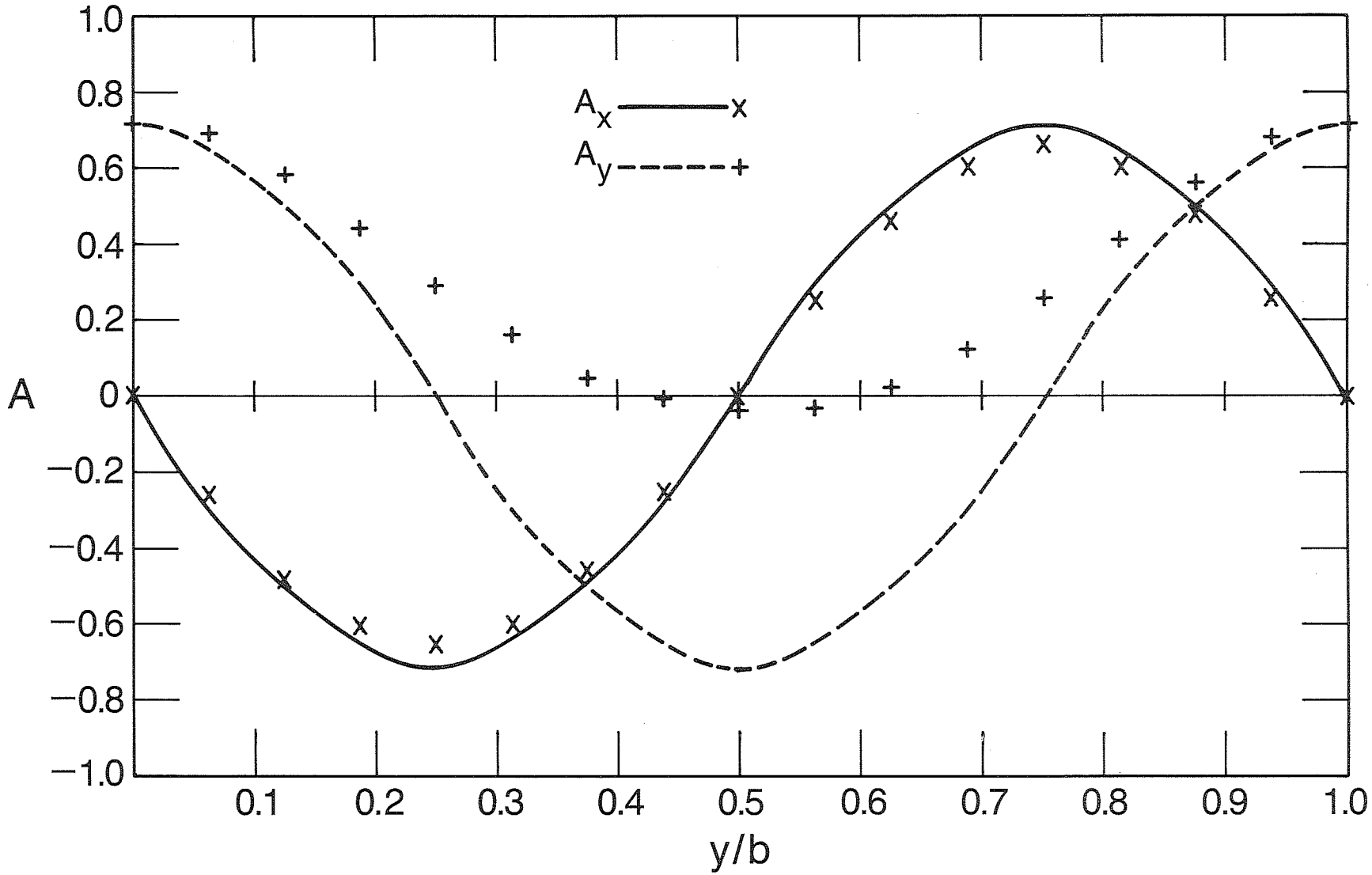

Figure 3-8 b) Comparison of computed results to TE_{123} fields when all components of $\vec{A}$ are fixed on the boundary. As functions of y for (x,z) = (a/4, c/2).

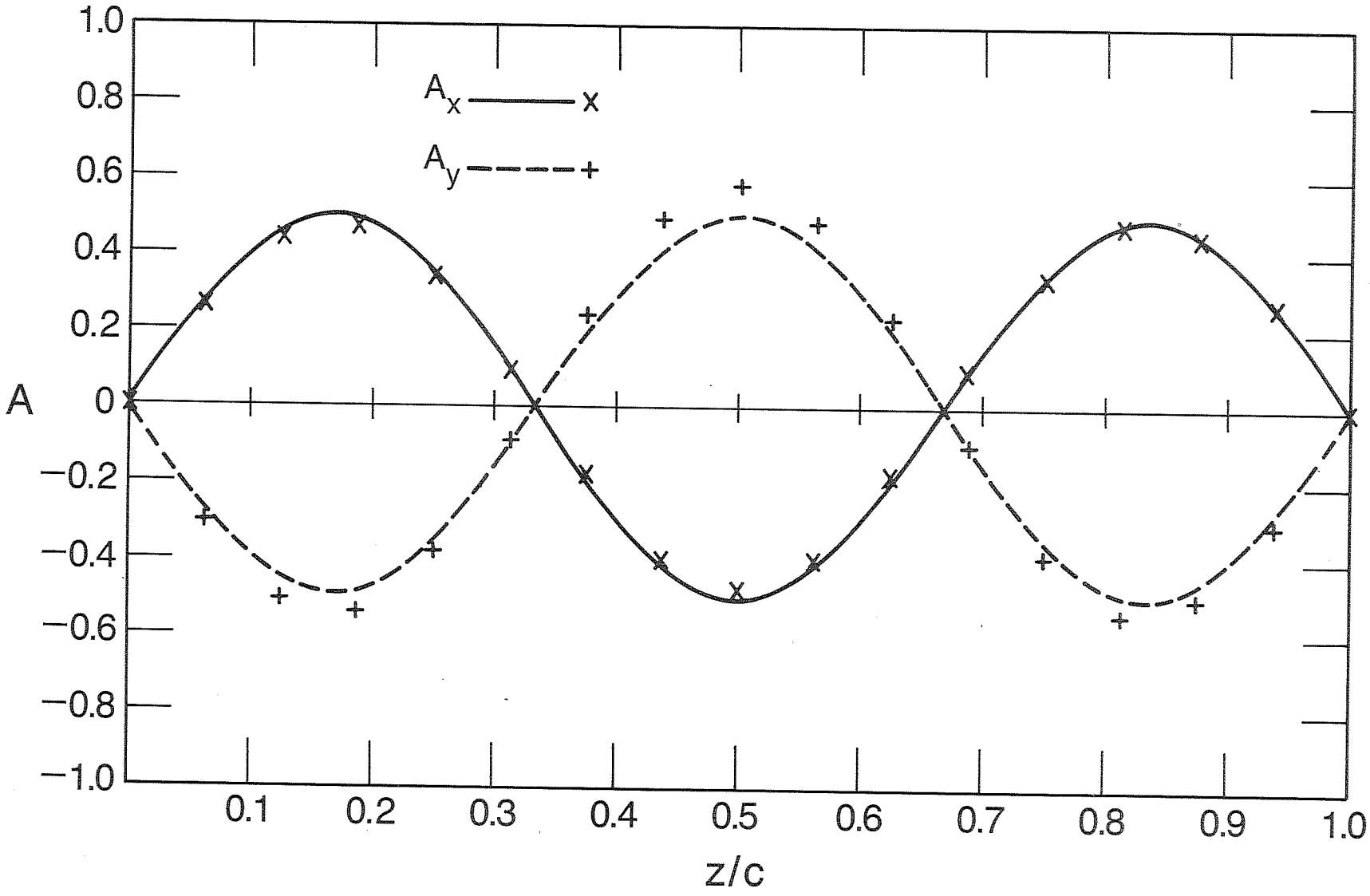

Figure 3-9 a) Comparison as in fig. 3-8. As functions of z for (x,y) = (a/4, b/8).

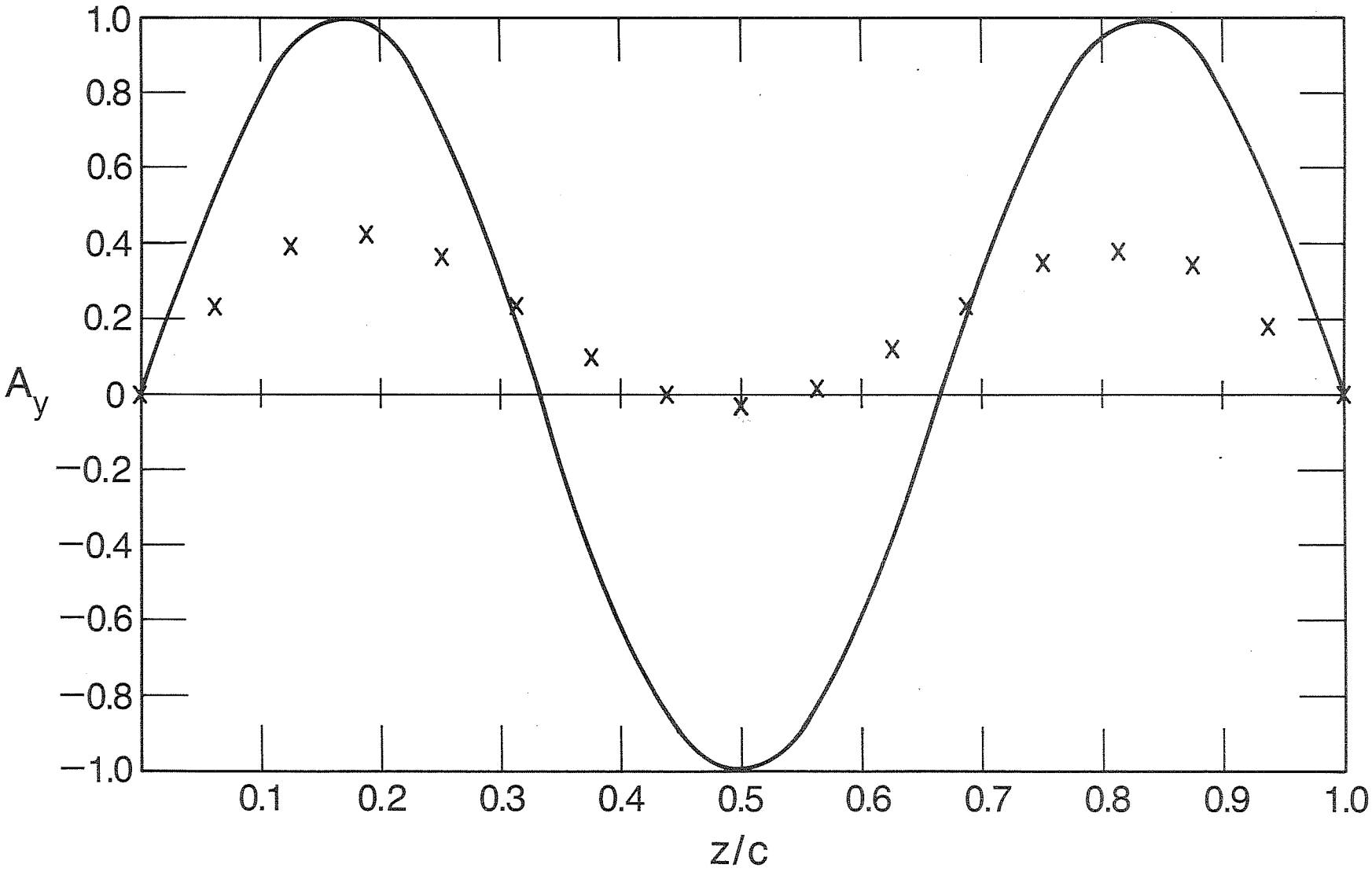

Figure 3-9 b) Comparison as in fig. 3-8. As functions of z for (x,y) = (a/2, b/2).

NBS-114A (REV. 2-80)

U.S. DEPT. OF COMM. BIBLIOGRAPHIC DATA SHEET (See instructions)	1. PUBLICATION OR REPORT NO. NBS/TN-1303	2. Performing Organ. Report No.	3. Publication Date October 1986

4. TITLE AND SUBTITLE

A LATTICE APPROACH TO VOLUMES IRRADIATED BY UNKNOWN SOURCES

5. AUTHOR(S)

J. Randa and M. Kanda

6. PERFORMING ORGANIZATION (If joint or other than NBS, see instructions)

NATIONAL BUREAU OF STANDARDS
DEPARTMENT OF COMMERCE
WASHINGTON, D.C. 20234

7. Contract/Grant No.

8. Type of Report & Period Covered

9. SPONSORING ORGANIZATION NAME AND COMPLETE ADDRESS (Street, City, State, ZIP)

10. SUPPLEMENTARY NOTES

☐ Document describes a computer program; SF-185, FIPS Software Summary, is attached.

11. ABSTRACT (A 200-word or less factual summary of most significant information. If document includes a significant bibliography or literature survey, mention it here)

We suggest an approach to the characterization of electromagnetic environments irradiated by unknown sources. The approach is based on the numerical solution of Maxwell's equations subject to the constraints imposed by the measured values of the field at a small number of measurement points and by boundary conditions. A thorough examination of two methods for the numerical solution is presented. The examples attempted demonstrate the approach but reveal that neither technique is fully successful. Possible future directions are suggested.

12. KEY WORDS (Six to twelve entries; alphabetical order; capitalize only proper names; and separate key words by semicolons)

electromagnetic environment characterization; electromagnetic environment effects; Hamilton's action principle; ill-posed problems; numerical methods; successive over-relaxation methods

13. AVAILABILITY

☒ Unlimited

☐ For Official Distribution. Do Not Release to NTIS

☒ Order From Superintendent of Documents, U.S. Government Printing Office, Washington, D.C. 20402.

☐ Order From National Technical Information Service (NTIS), Springfield, VA. 22161

14. NO. OF PRINTED PAGES

64

15. Price

*U.S. GOVERNMENT PRINTING OFFICE: 1986-0-773-597/65018

USCOMM-DC 6043-P80